

THE MAGNETIC MOMENT OF THE LAMBDA HYPERON

By LINDSAY CAROL SCHACHINGER

A thesis submitted to
The Graduate School
of
Rutgers, The State University of New Jersey
in partial fulfillment of the requirements
for the degree of
Doctor of Philosophy
Graduate Program in Physics

Written under the direction of
Professor Thomas J. Devlin
and approved by

New Brunswick, New Jersey

October 1978

ABSTRACT OF THE THESIS

The Magnetic Moment of the Lambda Hyperon

by LINDSAY CAROL SCHACHINGER, Ph. D.

Thesis Director: Professor Thomas J. Devlin

The magnetic moment of the lambda hyperon has been measured to be -0.6138 ± 0.0047 nuclear magneton. The experiment was performed in the neutral hyperon beam at the Fermi National Accelerator Laboratory. Three million $\Lambda^0 \rightarrow p \pi^-$ decays were detected in a multi-wire proportional chamber spectrometer. The lambda sample, produced inclusively by 400 Gev protons, had an average momentum of 114 Gev/c and an average polarization of 0.085. This polarization was precessed through angles as large as 153 degrees.

PREFACE

I would like to thank my thesis professor, Tom Devlin, for his constant optimism and infinite energy. His knack for stepping in at the moment of crisis with the perfect solution was invaluable. All the members of the Neutral Hyperon Group contributed to this project. Gerry Bunce, Ken Heller and Bob Handler were constant sources of advice. Tim Cox was an integral part of the magnetic field measurement. I am indebted to Lee Pondrom for his insight, encouragement, and enthusiasm. Many thanks also go to Jay Dworkin for a great SWIC cable and lots of moral support. Much of the equipment was built by G. Ott and E. Behr.

The staff of the Meson Lab aided us throughout the experiment.

I would especially like to thank my family, without whose love and support this project could not have been completed.

TABLE OF CONTENTS

	page
ABSTRACT	ii
PREFACE	iii
TABLE OF CONTENTS	iv
LIST OF TABLES	vi
LIST OF FIGURES	vii
1. INTRODUCTION	1
1.1 Experimental Background	3
1.2 Theoretical Background	6
2. APPARATUS	14
2.1 Diffracted Proton Beam	14
2.2 The Hyperon Target and Associated Detectors	18
2.3 The Neutral Beam Collimator	21
2.4 Magnetic Measurements	22
2.5 The Spectrometer	32
2.6 Trigger Logic	33
2.7 Data Acquisition	35
2.8 Data Taking Conditions	36
3. DATA ANALYSIS	39
3.1 Reconstruction Program and Data Summary Tapes	39
3.2 Event Selection	41

3.3 The Polarization Analysis	51
3.4 Polarization and Experimental Biases	58
3.5 Precession Analysis	76
3.6 Systematic Effects and Backgrounds	84
3.7 Parity Violating Polarization	87
3.8 5 Mrad Polarization	87
4. RESULTS	90
4.1 Magnetic Moment	90
4.2 Polarization	90
4.3 Summary	96
APPENDIX. COORDINATE SYSTEM	97
REFERENCES	100
VITA	103

LIST OF TABLES

	page
1.1 The electron, muon, proton, and neutron magnetic moments.	2
1.2 The up, down, and strange quark quantum numbers.	7
1.3 The stable baryon SU(6) wavefunctions.	8
1.4 The stable baryon magnetic moments both measured and predicted.	11
1.5 The quark magnetic moments and masses.	12
2.1 The distribution of data tapes written.	38
4.1 The Λ^0 magnetic moment, polarization, and biases as a function of momentum.	91
4.2 The z parity violating polarization.	93
4.3 The y parity violating polarization.	94
4.4 The 5 mrad polarization.	95
A.1 The angles through which the proton beam is bent.	99

LIST OF FIGURES

	page
1.1 A comparison of previous μ_{Λ} measurements with this measurement.	5
1.2. The SU(6) octet $J^P=1/2^+$ baryons.	9
2.1 The M2 beam line.	17
2.2 The experimental apparatus.	15
2.3a The hyperon target and associated detectors and collimator.	19
2.3b An elevation view of the sweeping magnet aperture.	20
2.4 The field map for $\int Bdl=13.64$ T-m.	24
2.5 Field integral versus sweeper current.	29
2.6 Field integral versus the standard field.	30
2.7 The electronic logic.	34
3.1 The p- π invariant mass.	43
3.2 The Λ^0 momentum spectrum.	44
3.3 The acceptance for Λ^0 , $\bar{\Lambda}^0$, and K_S^0 as a function of momentum.	45
3.4 The Λ^0 decay vertex distribution.	48
3.5 R^2 at the production target.	49
3.6 The angle with respect to the z axis in the y-z plane for Λ^0 's.	50
3.7 χ^2 per degree of freedom distribution for	

fits of Monte Carlo $\cos \theta^{\circ}$ distributions to real event $\cos \theta^{\circ}$ distributions.	54
3.8 χ^2 per degree of freedom distribution for fits of Monte Carlo geometric distributions to real event distributions.	57
3.9 The Λ° polarization as a function of momentum.	59
3.10 An illustration of the Λ° spin precession in the sweeping field.	60
3.11 The biases versus momentum for 7.2 mrad.	62
3.12 The z bias versus momentum.	66
3.13 The 0 mrad polarizations.	67
3.14 The 7.2 mrad y polarization.	71
3.15 The x and z biases for 0, 5, and 7.2 mrad.	72
3.16 The x and z biases for all field integrals.	74
3.17 The precession angle versus field integral.	77
3.18 The x and z spectrometer magnet biases.	80
3.19 The magnetic moment versus Λ° momentum.	83
3.20 The parity violating polarization.	88
3.21 The 5 mrad polarization.	89

CHAPTER 1

INTRODUCTION

Magnetic moments have played a major role in the development of our current understanding of the microscopic structure of matter. The Zeeman effect and the Stern-Gerlach experiment were crucial to modern ideas of angular momentum, spin, quantum mechanics, and atomic structure. The magnetic moments of the deuteron and other nuclei shed light on the structure of these composite systems. Extraordinarily precise measurements of the magnetic moments of the electron and muon have supported the validity of quantum electrodynamics and established that these charged leptons are point-like Dirac particles.

A magnetic moment is defined

$$\vec{\mu} = \frac{ge}{2mc} \vec{s}$$

where \vec{s} is the spin. Magnetic moments are conventionally

expressed in units either of Bohr magnetons ($e\hbar/2m_e c = .57883785 \times 10^{-14}$ Mev/gauss) or nuclear magnetons (n.m. = $e\hbar/2m_p c = 3.1524515 \times 10^{-18}$ Mev/Gauss). Charged point-like spin 1/2 fermions like the electron and muon have $g=2$, neutral ones have $g=0$. Departure from these values implies some sort of internal structure. The electron, muon, proton, and neutron magnetic moments are given in table 1.1 for comparison.^{1,2,3} The baryons have large anomalous moments, and by measuring these precisely one hopes to gain some knowledge of their composition.

PARTICLE	MAGNETIC MOMENT
e	1.0011596567(35) $e\hbar/2m_e c$
μ	1.001166895(27) $e\hbar/2m_\mu c$
p	2.7928456(11) $e\hbar/2m_p c$
n	-1.913148(66) $e\hbar/2m_p c$

Table 1.1 The electron, muon, proton and neutron magnetic moments

1.1 EXPERIMENTAL BACKGROUND

The magnetic moment of the Λ^0 is measured by precessing the polarization vector of a Λ^0 sample in a magnetic field. The spin precesses according to the equation

$$\frac{d\vec{S}}{dt} = \vec{S} \times \vec{\Omega}$$

$$\vec{\Omega} = \frac{ge}{2m} [\vec{B} - \frac{\gamma-1}{\gamma} (\vec{B} \cdot \hat{p}_\Lambda) \hat{p}_\Lambda]$$

where B is the magnetic field, \hat{p}_Λ is a unit vector in the direction of the Λ^0 momentum in the laboratory, γ^2 is $1/(1 - (p/E)^2)$, $E^2 = p^2 + m^2$. If the Λ^0 momentum is perpendicular to the magnetic field, the Λ^0 spin precesses about the magnetic field

$$\frac{d\vec{S}}{dt} = \frac{ge}{2m} \vec{S} \times \vec{B}$$

If the spin is perpendicular to the magnetic field,

$$\left| \frac{d\hat{S}}{dt} \right| = \left| \frac{ge}{2m} \vec{B} \right|$$

Integrating this over the path of the Λ^0 in the magnetic field, the angle through which the spin precesses is

$$\theta = \frac{g e}{2 m \beta c} \int B dl$$

where $\int B dl$ is the integral of the magnetic field over the Λ^0 path.

So the magnetic moment ($g/2$) is obtained by measuring the angle through which the Λ^0 polarization vector precesses and the magnetic field integral over the Λ^0 path.

Before 1976, measurements of the magnetic moment of the Λ^0 were done using Λ^0 's produced in the reaction $\pi + N \rightarrow \Lambda^0 + K$ at 1 Gev.⁸⁻¹³ The Λ^0 's from this reaction are 100% polarized perpendicular to the plane of the Λ^0 and K. The cross section for this reaction is small and the average flight path of the Λ^0 's is short (7 cm) necessitating the use of large (200 kG) pulsed magnetic fields to obtain precession angles of a few degrees.

In 1976, it was discovered in the neutral hyperon beam at Fermilab that Λ^0 's produced inclusively in the reaction $p + Be \rightarrow \Lambda^0 + X$ at 300 Gev were polarized.¹⁴ The Λ^0 polarization was perpendicular to the production plane and increased with the Λ^0 transverse momentum to 0.20 at $p_t = 2$ Gev/c. This phenomenon has since been reported at the CERN PS where the incident proton energy was 24 Gev.¹⁵ This discovery facilitated the measurement of the

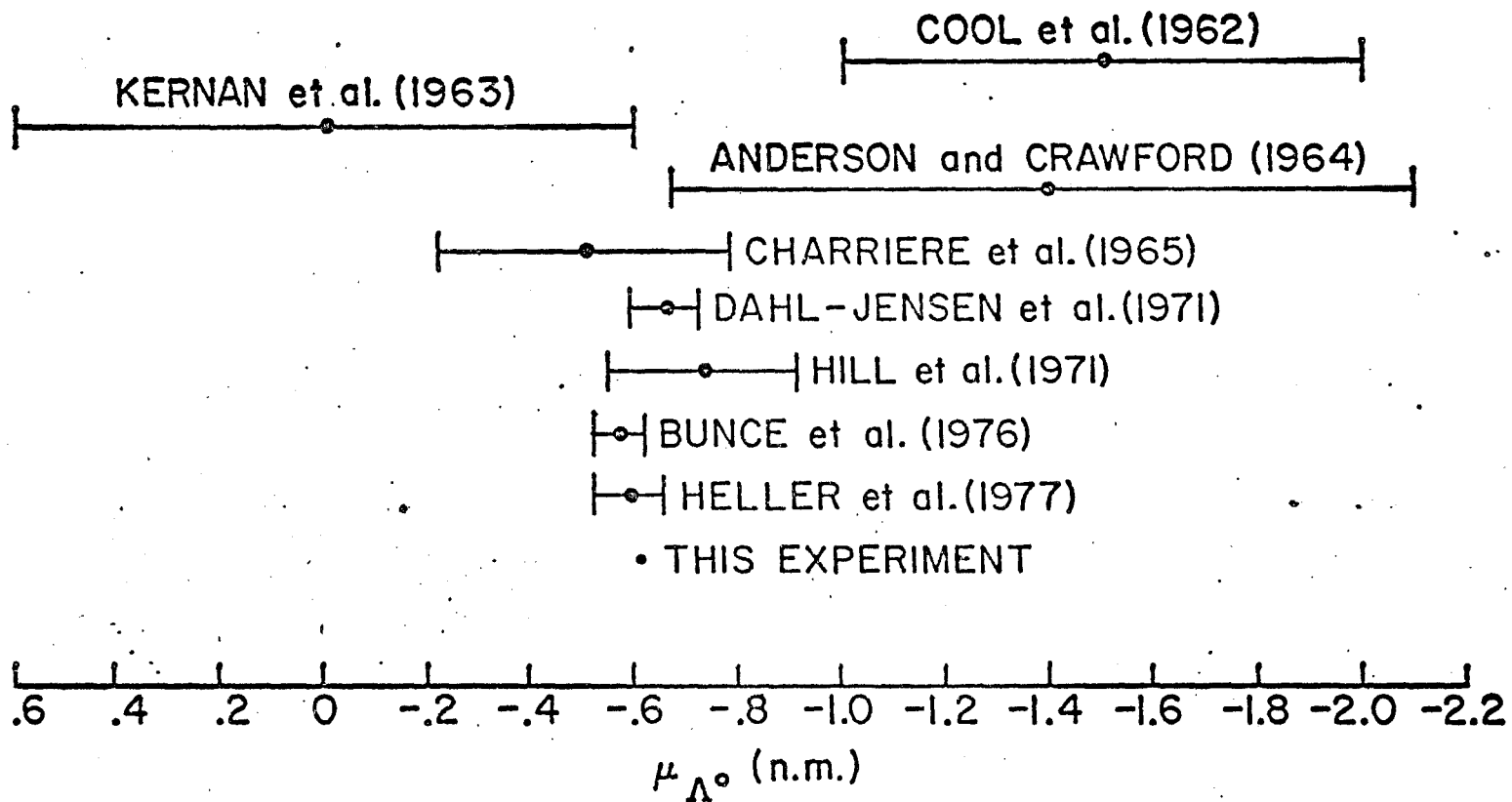


Figure 1.1 A comparison of previous μ_{Λ} measurements with this measurement.

Λ^0 magnetic moment by providing a source of high energy polarized Λ^0 's with a long (7 m) average flight path, whose spin therefore could be precessed through angles greater than 90 degrees with conventional magnetic fields. A large inclusive cross section also allowed 3×10^6 Λ^0 decays to be collected in 60 hours of data taking. Figure 1.1 shows a comparison of the previous measurements of the moment with this measurement. Bunce et al. and Heller et al. are the two previous measurements done with inclusively produced Λ^0 's.

Through the discovery of inclusive Λ^0 polarization increased precision in the measurement of the Λ^0 magnetic moment is possible, and it is this improved measurement which will be reported here.

1.2 THEORETICAL BACKGROUND

One successful model for the internal structure of hadrons is SU(6) and the quark model. The hadrons in this model are composed of three types of quarks u, d, and s whose quantum numbers are given in table 1.2.

	u	d	s
q/e	2/3	-1/3	-1/3
I ₃	1/2	-1/2	0
S	0	0	-1

Table 1.2 The up, down, and strange quark quantum numbers

Baryons in this model are formed of 3 quarks, mesons of a quark and an anti-quark. The quark composition of the stable baryons is given in table 1.3 and the quantum numbers of the spin 1/2 positive parity baryons are displayed in figure 1.2.¹⁶ The Λ^0 is made of a u and a d quark in a spin singlet and an isospin singlet state, and an s quark. Thus the spin of the Λ^0 is the spin of its s quark. No other particle has this property.

The magnetic moments of the baryons can be written as the sums of the magnetic moments of the constituent quarks,

$$\mu_B = \sum_i \langle B | \mu_i | B \rangle$$

where $|B\rangle$ represents the SU(6) wavefunction. If

$\mu_i = q_i \hbar / 2m_0 c = q_i \mu_0$, the symmetry is exact and the $J^P = 1/2^+$

BARYON	3 x SU(6) WAVEFUNCTION (perm. omitted)
p	$\sqrt{2/3} u\uparrow u\uparrow d\downarrow - \sqrt{1/3} (u\uparrow u\downarrow + u\downarrow u\uparrow) d\uparrow / \sqrt{2}$
n	$\sqrt{2/3} d\uparrow d\uparrow u\downarrow - \sqrt{1/3} (d\uparrow d\downarrow + d\downarrow d\uparrow) u\uparrow / \sqrt{2}$
Σ^+	$\sqrt{2/3} u\uparrow u\uparrow s\downarrow - \sqrt{1/3} (u\uparrow u\downarrow + u\downarrow u\uparrow) s\uparrow / \sqrt{2}$
Σ^0	$\sqrt{2/3} u\uparrow d\uparrow s\downarrow - \sqrt{1/3} (u\uparrow d\downarrow + u\downarrow d\uparrow) s\uparrow / \sqrt{2}$
Σ^-	$\sqrt{2/3} d\uparrow d\uparrow s\downarrow - \sqrt{1/3} (d\uparrow d\downarrow + d\downarrow d\uparrow) s\uparrow / \sqrt{2}$
Ξ^0	$\sqrt{2/3} s\uparrow s\uparrow u\downarrow - \sqrt{1/3} (s\uparrow s\downarrow + s\downarrow s\uparrow) u\uparrow / \sqrt{2}$
Ξ^-	$\sqrt{2/3} s\uparrow s\uparrow d\downarrow - \sqrt{1/3} (s\uparrow s\downarrow + s\downarrow s\uparrow) d\uparrow / \sqrt{2}$
Λ^0	$(u\uparrow d\downarrow - u\downarrow d\uparrow) s\uparrow / \sqrt{2}$
Ω^-	$s\uparrow s\uparrow s\downarrow$

Table 1.3 The stable baryon SU(6) wavefunctions

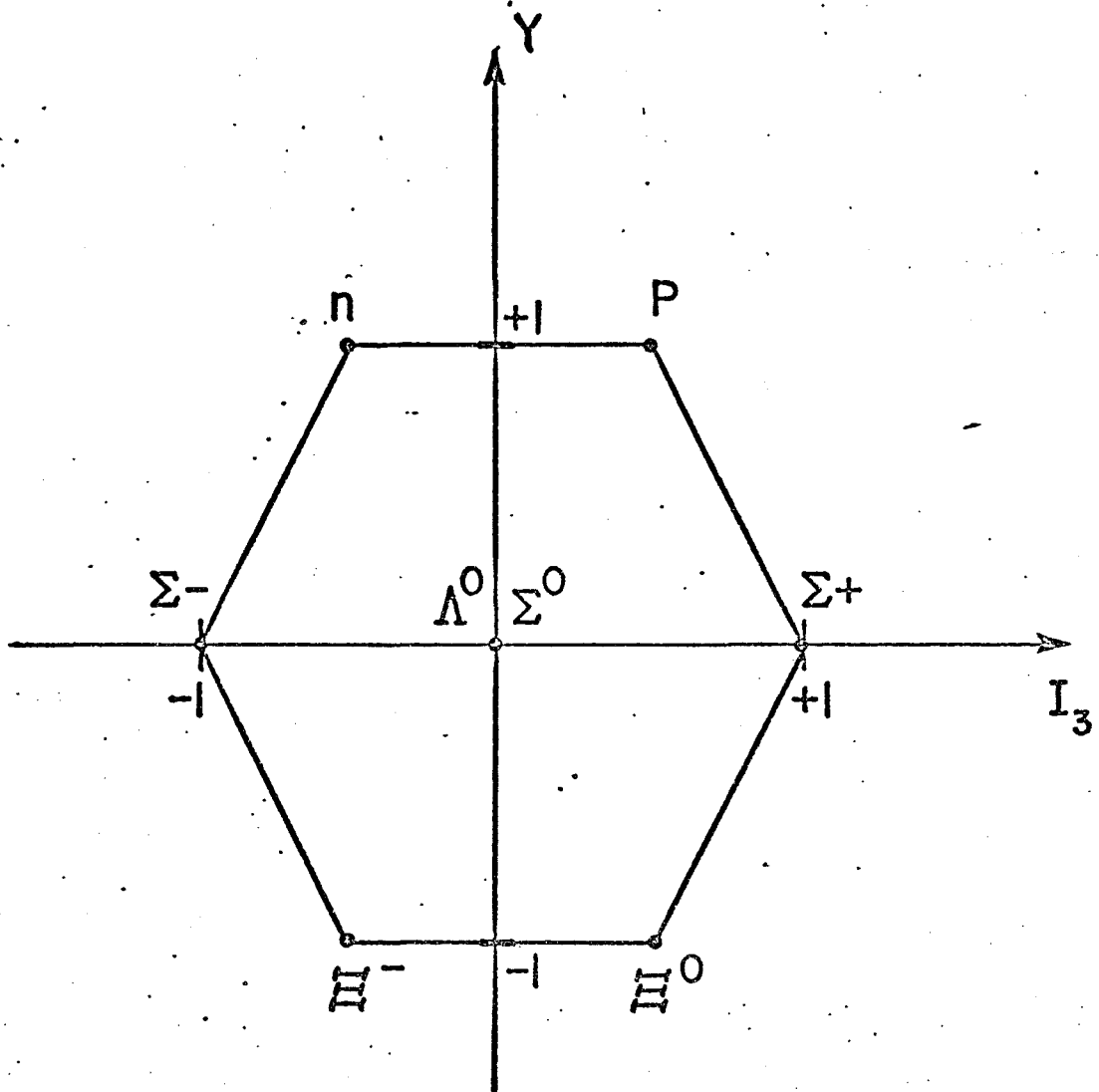


Figure 1.2 The SU(6) Octet $J^P = 1/2^+$ Baryons.

baryon magnetic moments are given in table 1.4. Although the ratio of the proton and neutron moments in this simple picture agrees with experiment to a few percent, the Λ^0 moment does not. However, if we break the SU(6) symmetry by allowing the s quark to be more massive than the u or d quarks, and take $\mu_i = q_i \hbar / 2m_i c$ with $m_u = m_d$, the results are

$$\begin{aligned}\mu_p &= \frac{4}{3}\mu_u - \frac{1}{3}\mu_d \\ \mu_n &= \frac{4}{3}\mu_d - \frac{1}{3}\mu_u \\ \mu_\Lambda &= \mu_s\end{aligned}$$

The three measured moments μ_p , μ_n , and μ_Λ define the three parameters μ_u , μ_d , and μ_s , listed in table 1.5. The quark masses, calculated from the moments assuming $g=2$ for quarks ($m_q = m_p q_q / \mu_q e$) are also listed in table 1.5. All other magnetic moments and the magnetic dipole transition $\Sigma^0 \rightarrow \Lambda^0 \gamma$ can be calculated using the wavefunctions of table 1.3 and the three quark moments. This calculation yields the results in the third column of table 1.4 which agree well with the experimental measurements.⁴⁻⁷ More precise measurements are necessary to test these predictions at the 2-3 per cent level at which they seem to be valid.

BARYON	MAGNETIC MOMENT (n.m.)		
	EXPERIMENT	EXACT SU(6)	BROKEN SU(6)
p	2.79	input	input
n	-1.91	-1.86	input
Λ^0	-0.6138 ± 0.0047	-0.93	input
Σ^+	2.95 ± 0.31	2.79	2.673
Σ^0	-----	0.93	0.790
Σ^-	-1.48 ± 0.37	-0.93	-1.091
Ξ^0	-----	-1.86	-1.435
Ξ^-	-1.85 ± 0.75	-0.93	-0.494
$ \Sigma^0 \rightarrow \Lambda^0 \delta $	$1.82^{+0.25}_{-0.18}$	1.66	1.630
Ω^-	-----	-2.79	-1.840

Table 1.4. The stable baryon magnetic moments both measured and predicted.

QUARK	μ (n.m.)	MASS (Mev/c ²)
u	1.852	358
d	-0.972	322
s	-0.614	509

Table 1.5 The quark magnetic moments and masses

The quark masses can be determined independently in several ways, the simplest of which is

$$m_u = m_d = m_n/3 = 313 \text{ Mev}/c^2$$

$$m_s = m_\Lambda - 2m_u = 490 \text{ Mev}/c^2$$

which agree with the values in table 1.5 to 7%. Multiplet splittings can also be used to determine $m_u/m_s=0.62$, yielding $\mu_\Lambda=-0.6$ n.m..¹⁷ The bag model prediction ($m_u=m_d=0$, $m_s=300 \text{ Mev}/c^2$) is also -0.6 n.m..¹⁸ The agreement between the quark masses calculated from their moments and the masses calculated from particle masses implies that the assumption that $g=2$ for quarks is valid.

This measurement of the Λ^0 magnetic moment is therefore in good agreement with broken SU(6) predictions. Assuming the s quark is a point-like spin

1/2 fermion the value $\mu_{\Lambda} = -0.6138 \pm 0.0047$ n.m. implies $m_s = 509 \pm 4$ Mev/c². Using μ_p , μ_n , and μ_{Λ} , the other baryon moments can be calculated, and remain to be more precisely measured.

CHAPTER 2

APPARATUS

The experiment was performed in the neutral hyperon beam in the M2 diffracted proton beam at Fermilab. The apparatus, shown in figure 2.2, is described in detail elsewhere.¹⁹⁻²¹ The basic components of the apparatus were a Be target, a magnetized collimator which defined the neutral beam, an evacuated decay region, and a spectrometer which consisted of six multi-wire proportional chambers and a spectrometer magnet with a transverse bending power of 0.7266 Gev/c. The wire chamber data were read into the on-line PDP-11/45 computer memory through a CAMAC interface and written to magnetic tape for each event.

2.1 DIFFRACTED PROTON BEAM

ELEVATION VIEW

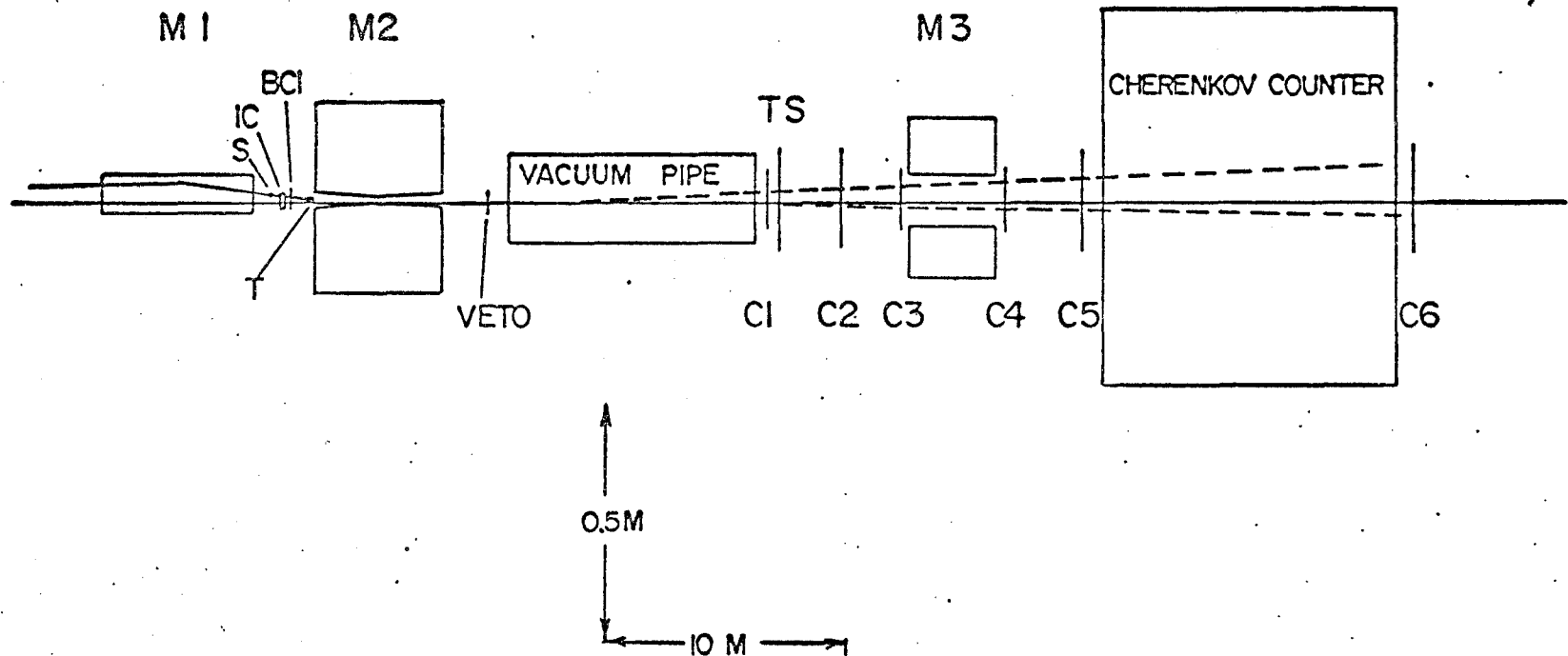


Figure 2.2 The experimental apparatus. M1 is the production target bending magnet, M2 is the sweeping/precession magnet, and M3 is the spectrometer magnet. S, IC, BC1, and T are shown in more detail in figure 2.3a.

During the experimental run the Fermilab synchrotron was operated at 400 Gev at intensities of approximately 2×10^{13} protons per machine cycle under typical conditions. The synchrotron delivered beam to the experimental areas every 15 seconds, in the form of a 2 second long spill.

The extracted proton beam was incident upon the Meson Lab production target, producing six secondary beams. One of these, the M2 diffracted proton beam was produced at 1 milliradian (mrad), and was transported to the experimental area through two stages, each consisting of two quadrupoles and one bending string. The beam elements are shown in figure 2.1. The main bends were horizontal.

In the following discussion all distances along the beam line are relative to the Meson Lab production target. The first stage produced a vertical and horizontal focus at 201 m. The second stage produced a focus at the experimental production target, at 451 m. A segmented wire ion chamber (SWIC) was located at 201 m to monitor the beam position and spot size at the focus. The intensity was varied with horizontal and vertical collimators, to a maximum of $>10^9$.

During the bulk of the data taking, the M2 diffracted proton beam was operated at an intensity of 2×10^8 protons per pulse at 400 Gev. A dipole magnet at 335 m bent the proton beam vertically through as much as 0.33 mrad. This produced a displacement above or below the median plane as large as 3.7 cm at the dipole magnet located at 446 m. The beam was restored by this magnet to the hyperon production target in the median plane at 451 m. In this manner, vertical production angles as large as 7.2 mrad, both positive and negative, were obtained. All the data used to measure the magnetic moment were taken at ± 7.2 mrad, and some data at 0 and ± 5 mrad were taken as experimental checks. A SWIC with 1 mm wire spacing was placed 91.3 cm upstream of the hyperon production target center. This SWIC was used to insure that the beam quality was constant and the beam displacement symmetric about 0 for positive and negative production angles.

2.2 THE HYPERON TARGET AND ASSOCIATED DETECTORS

The hyperon production target was a 15 cm long, 0.635 cm diameter beryllium cylinder. An Argon filled ion chamber which monitored the intensity of the proton beam was 104.9 cm upstream of the Be target center. A

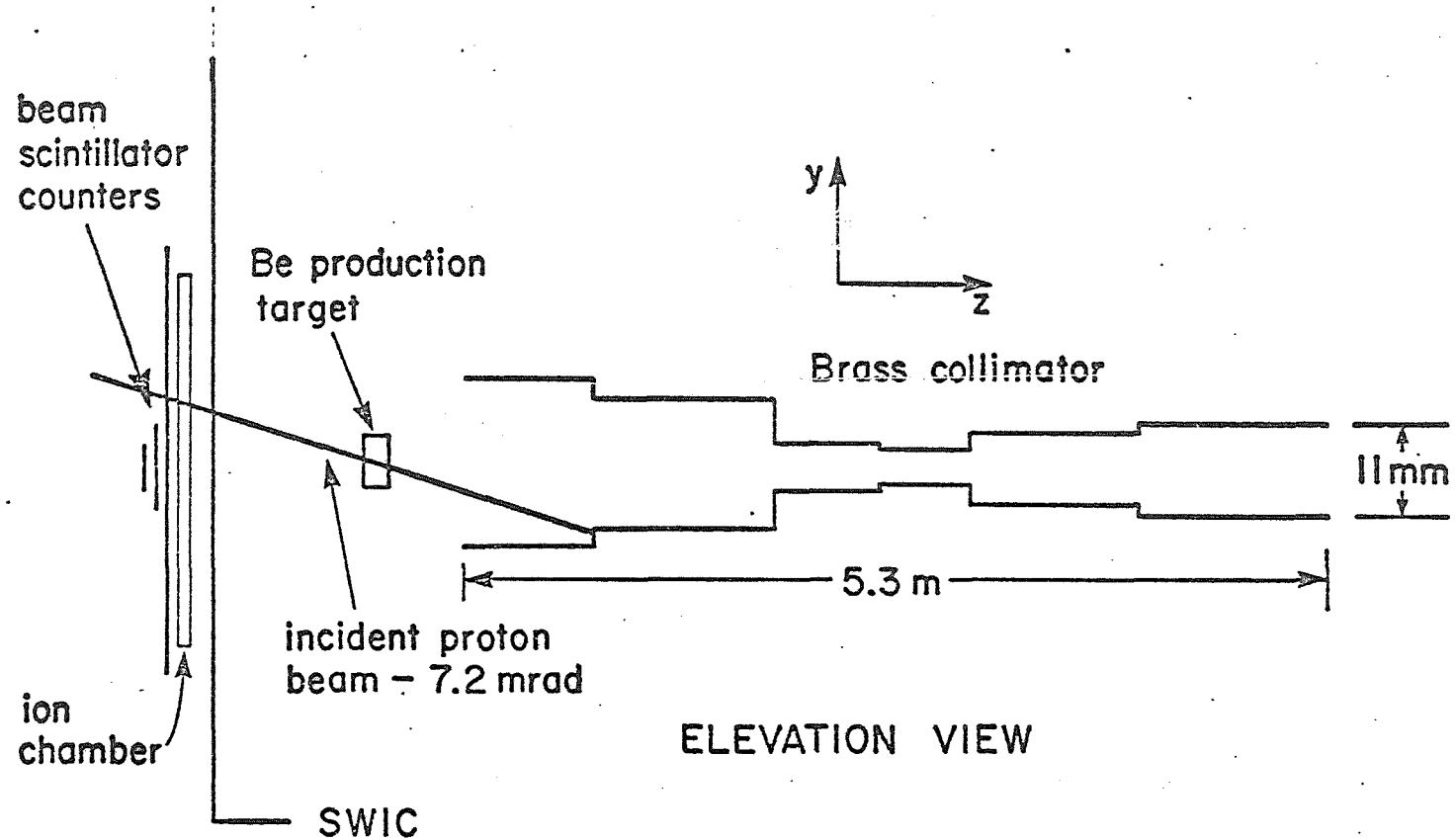


Figure 2.3a The hyperon production target and associated detectors and the collimator.

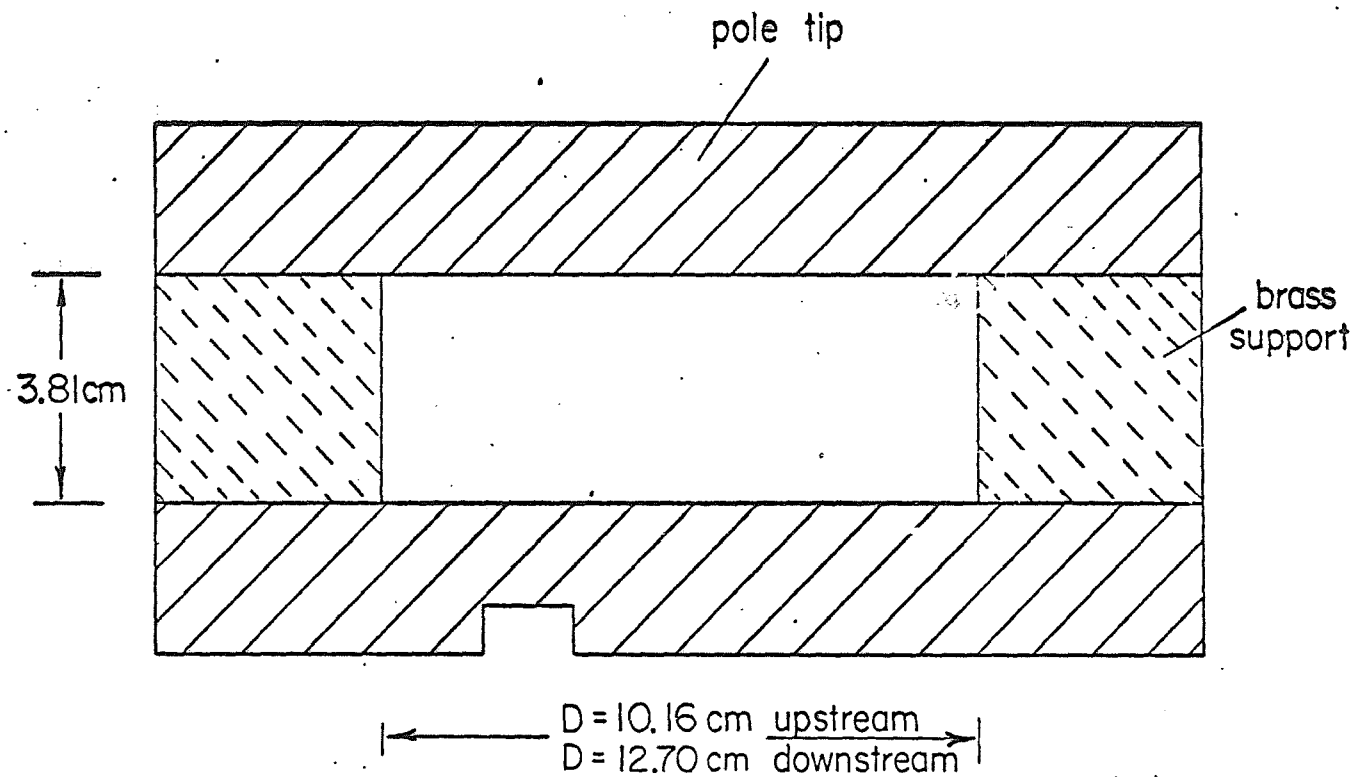


Figure 2.3b An elevation view of the sweeping magnet aperture.

set of three scintillators which monitored the quality of the proton beam focus and which were used to calibrate the ion chamber were located 122 cm upstream of the Be target center. None of these detectors were essential to the magnetic moment measurement. They are shown in figure 2.3a.

2.3 THE NEUTRAL BEAM COLLIMATOR

The production target was followed by a 5.3 m long magnetic channel which removed charged particles and defined the neutral beam. The field in this channel was vertical and had a maximum value of 2.5 Tesla. It also served as the precession field for the magnetic moment measurement.

Imbedded in this magnet was a brass collimator, illustrated in figure 2.3. At an incident angle of 7.2 mrad, the proton beam was buried in the second collimator block. The defining aperture was 4 mm in diameter, and the solid angle accepted was 1.2μ steradians. The collimator consisted of 6 brass blocks either 3.81x10.16 cm or 3.81x12.70 cm transverse to the beam direction, each with a different size aperture. These blocks were removable, to allow magnetic measurements to be performed

in the channel.

2.4 MAGNETIC MEASUREMENTS

Since the field integral in the sweeping magnet was directly involved in the measurement of the magnetic moment, it was necessary to measure it precisely. This was done in two ways. First a Nuclear Magnetic Resonance (NMR) probe and a Hall probe were used to map the magnetic field and the field integral was calculated. Second, a stretched wire probe was flipped in the field, giving a direct measurement of the field integral. During these measurements and during data taking an NMR probe in a fixed position in the collimator was used to set the field and to monitor its stability. The position of the probe was 112.55 cm from the downstream end of the last collimator block, 1.2 cm below beam height.

The field map was done with an NMR probe mounted at beam height in the magnet aperture, and with collimator blocks removed. Wherever the field inhomogeneity was such that the NMR probe could not be used, a Hall probe calibrated against the NMR probe was used. The field value was recorded every inch for two field integral values, 13.64 Tesla-meters and 11.22 T-m, for both field

polarities. The field map for 13.64 T-m is shown in figure 2.4. The precision of the NMR probe was 0.01%, and the Hall probe, which was used to measure 7% of the field integral, had 1% precision. The reproducibility of any point on the map was 0.01% for the NMR points and 1% for the Hall probe points. This includes the error in the field due to the error in the position of the probe. The overall uncertainty of this measurement, dominated by the Hall probe uncertainty, was 0.07%.

The stretched wire probe consisted of 2 turns of 0.0102 cm Tungsten wire 1.27 cm wide and 7.73 m long under 19.6 Newtons tension, positioned at beam height in the center of the magnet aperture. The spacing of the wires was achieved with quartz rods whose diameter was 1.27 cm \pm 0.04%. An integrator with a time constant of 0.1 second ($R=100k\Omega$, $C=1\mu f$) integrated the emf induced in the wires when they were flipped in the field region. The voltage output of the integrator was read by an electrometer. The field integral was

$$\int B dl = \frac{VRC}{2NW}$$

where N is the number of turns of wire, W is the width of the probe, V is the voltage output of the integrator, and RC is the integrator time constant. This measurement was

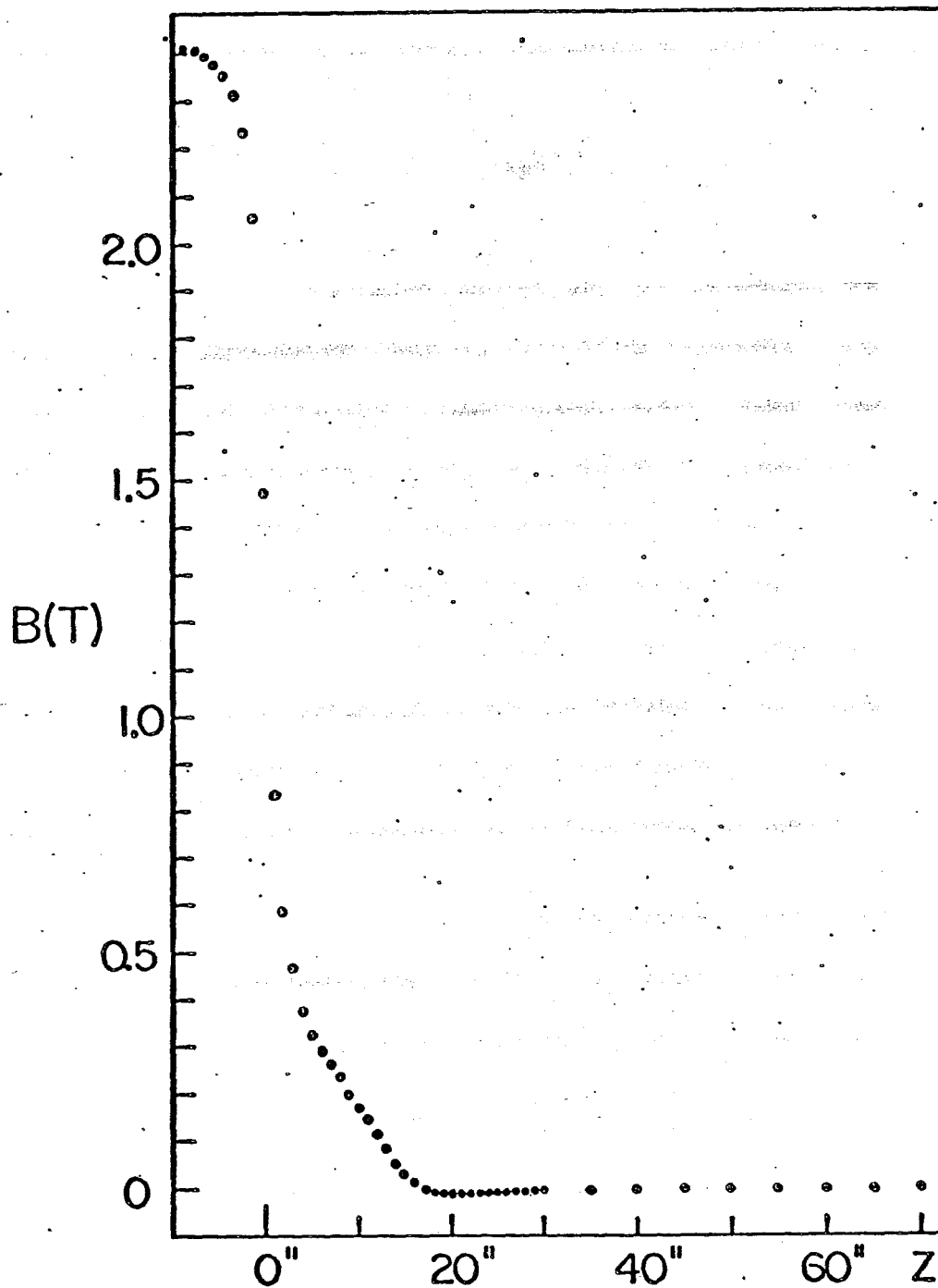


Figure 2.4a Field map for $\int Bdl = 13.64$ T-m.

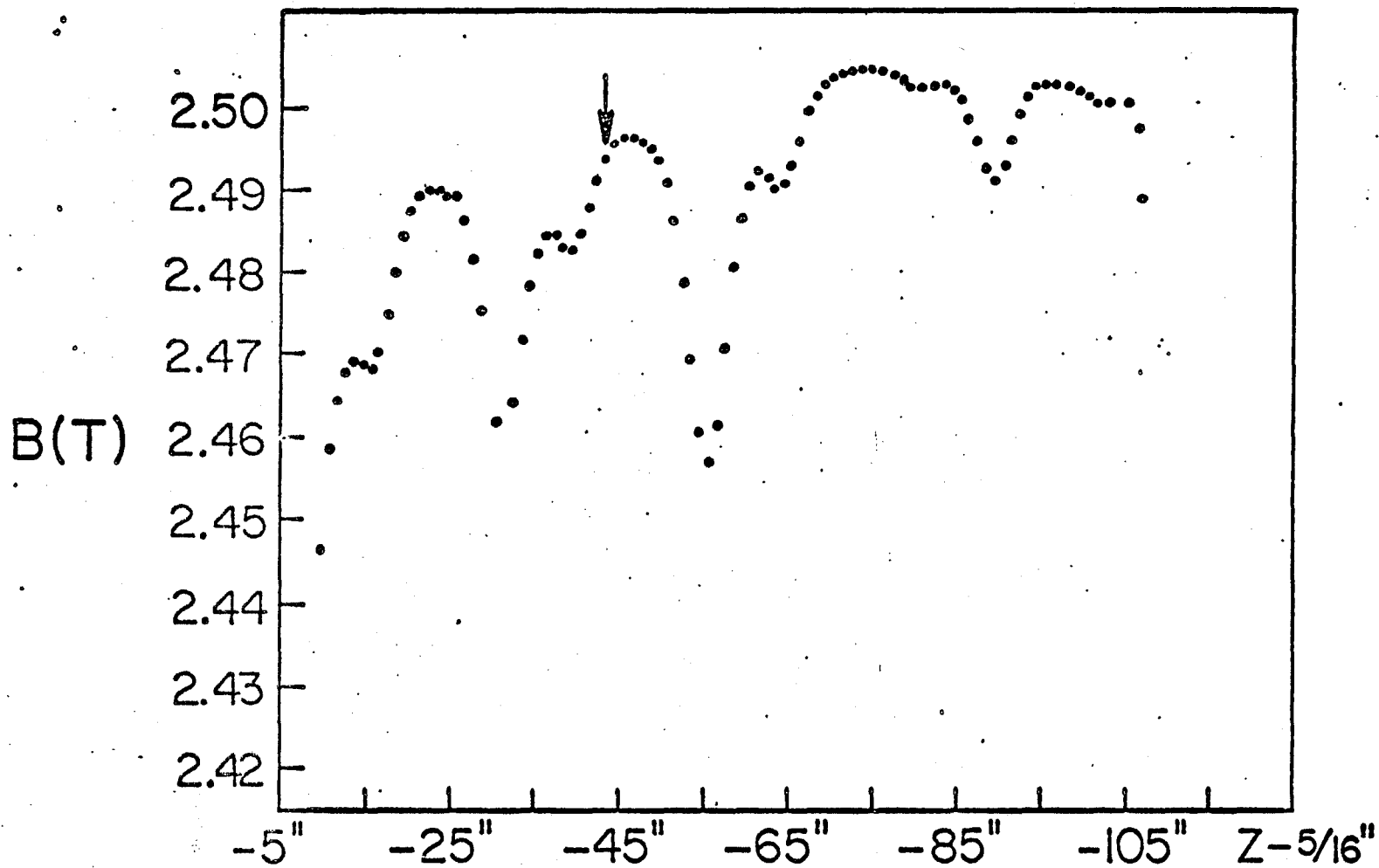


Figure 2.4b The field map for $\int B dl = 13.64$ T-m. The arrow indicates the position of the standard field.

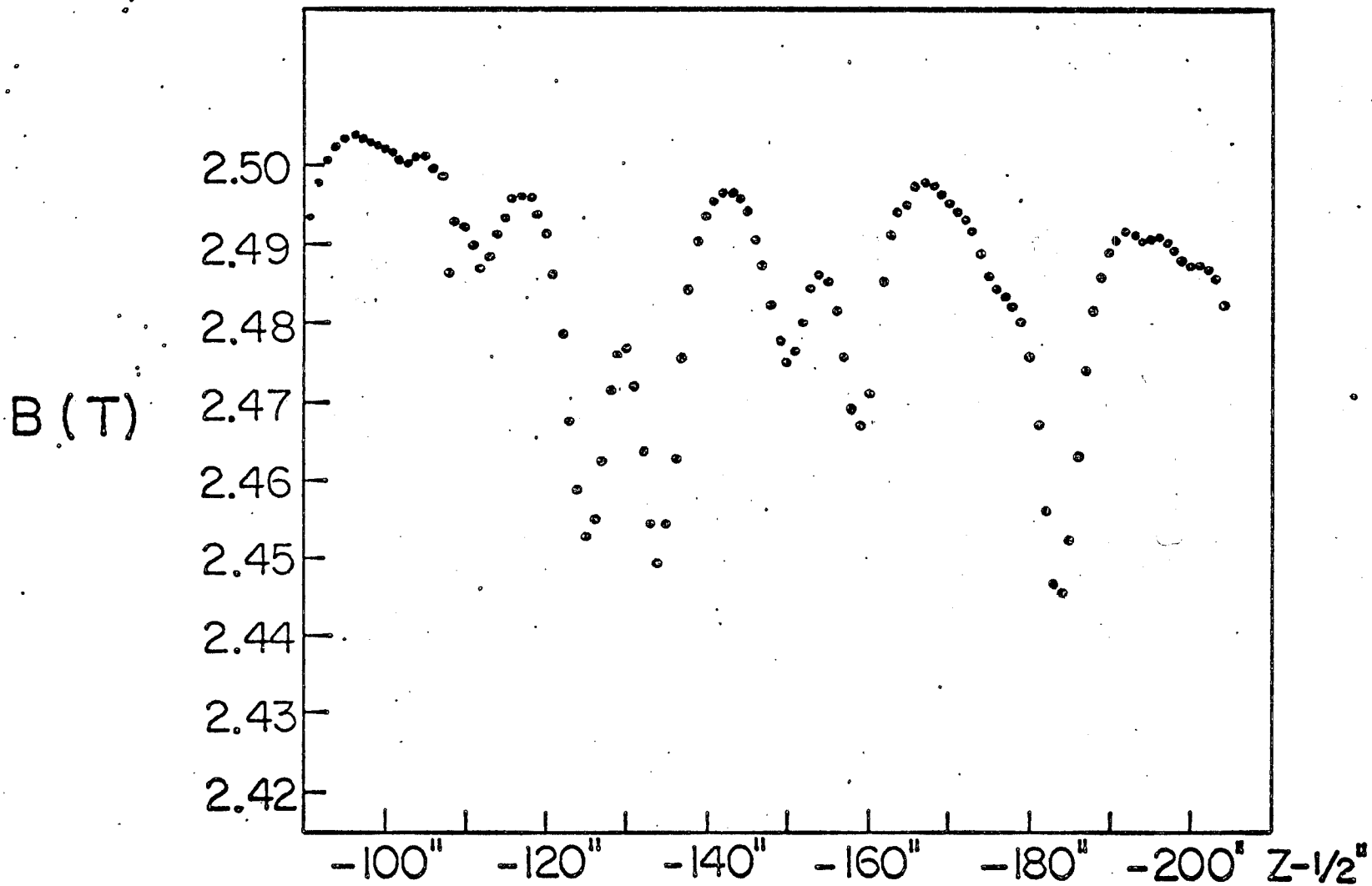


Figure 2.4e The field map for $\int B dl = 13.64$ T-m.

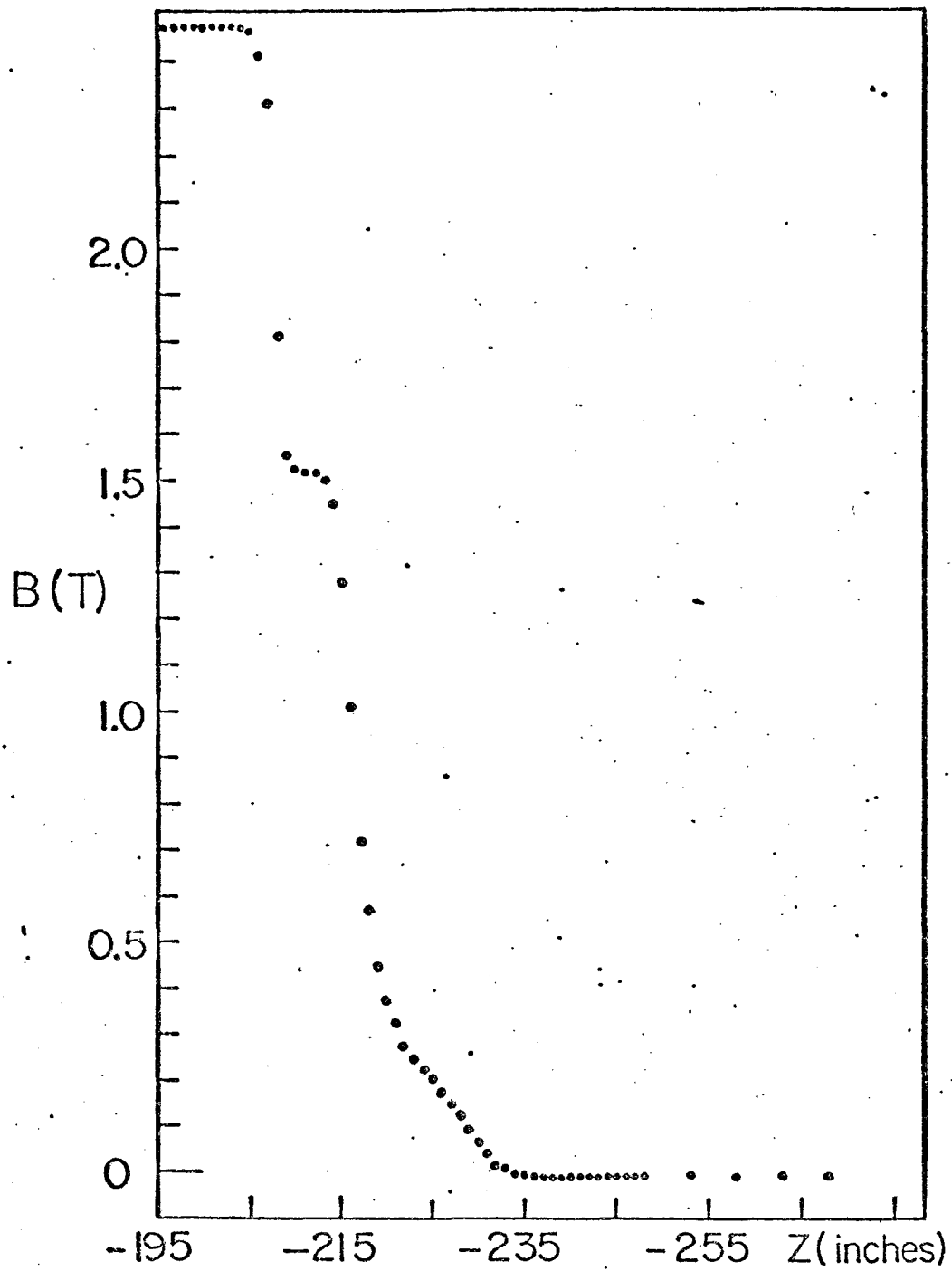


Figure 2.4d The field map for $\int Bdl=13.64$ T-m. The minima are due to air gaps between the iron plates.

performed for several field integral values, with the NMR probe in the standard position in the collimator for those fields within the frequency range of the NMR probe (above 1.5 Tesla). Figures 2.5 and 2.6 show the results of these measurements, when the stretched wire probe is calibrated against the NMR and Hall probe results. Before calibrating the stretched wire probe, the two methods agreed within the known 1% uncertainty in RC. With the calibration, the precision of the stretched wire method was 0.2% limited by integrator drift.

The stretched wire method was also used to check the uniformity of the field integral over the magnet aperture. The quartz rods holding the probe were mounted on lathe beds, and the position of the probe within the aperture was set at ± 1.02 cm and ± 2.54 cm horizontally and ± 0.51 cm vertically. For a horizontal displacement of ± 2.54 cm the field integral dropped to 99.8% of its value in the center of the aperture. The other positions showed no detectable difference from the center value. The maximum displacement from the center of the aperture for a Λ^0 produced at the target was 0.55 cm and the maximum angle with respect to the collimator axis was 1.5 mrad. Thus, there was no variation in field integral over the possible paths of target produced Λ^0 's through the collimator within the measurement errors.

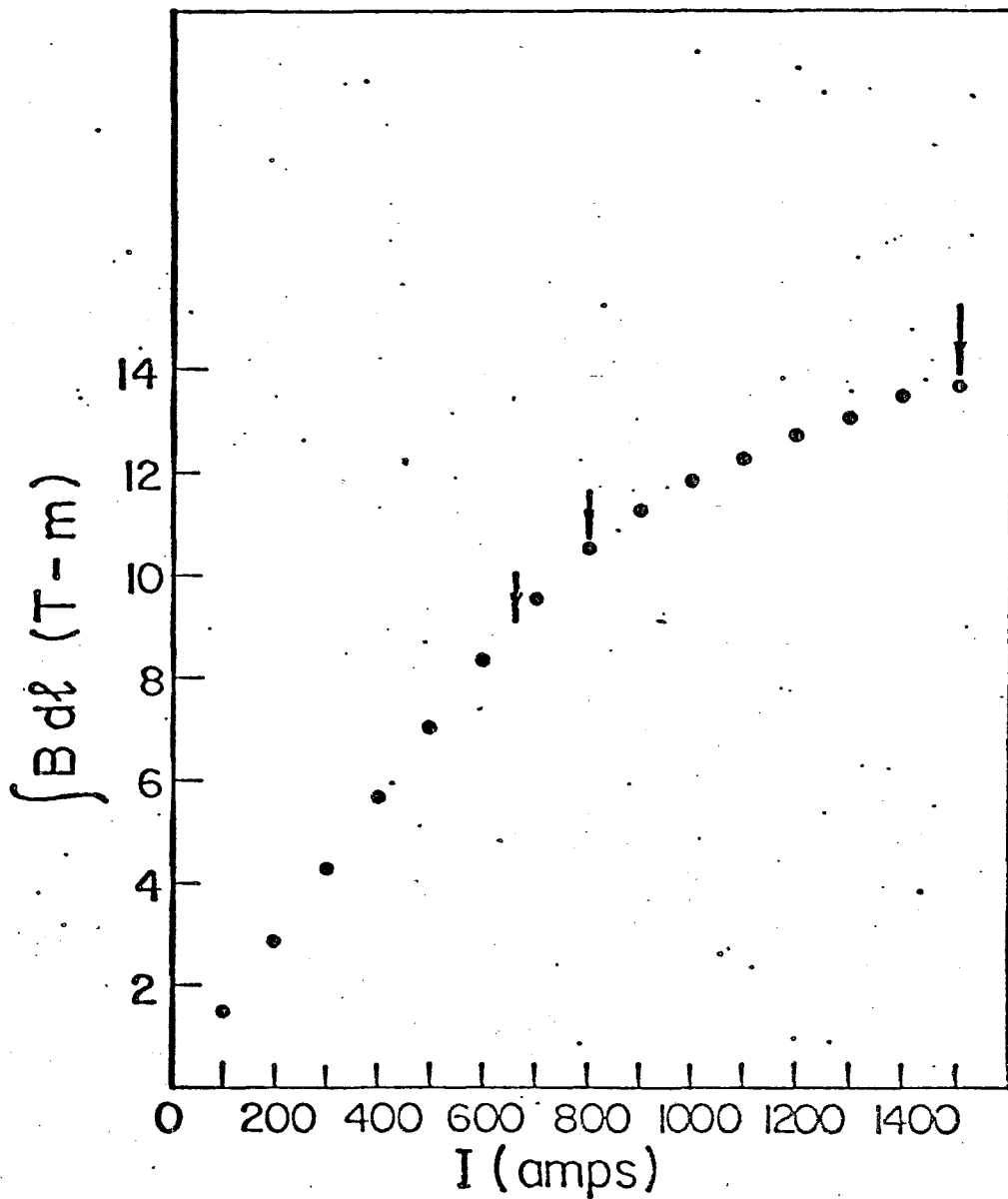


Figure 2.5 Field integral vs. sweeper current. The arrows indicate the non-zero field integrals at which data were taken.

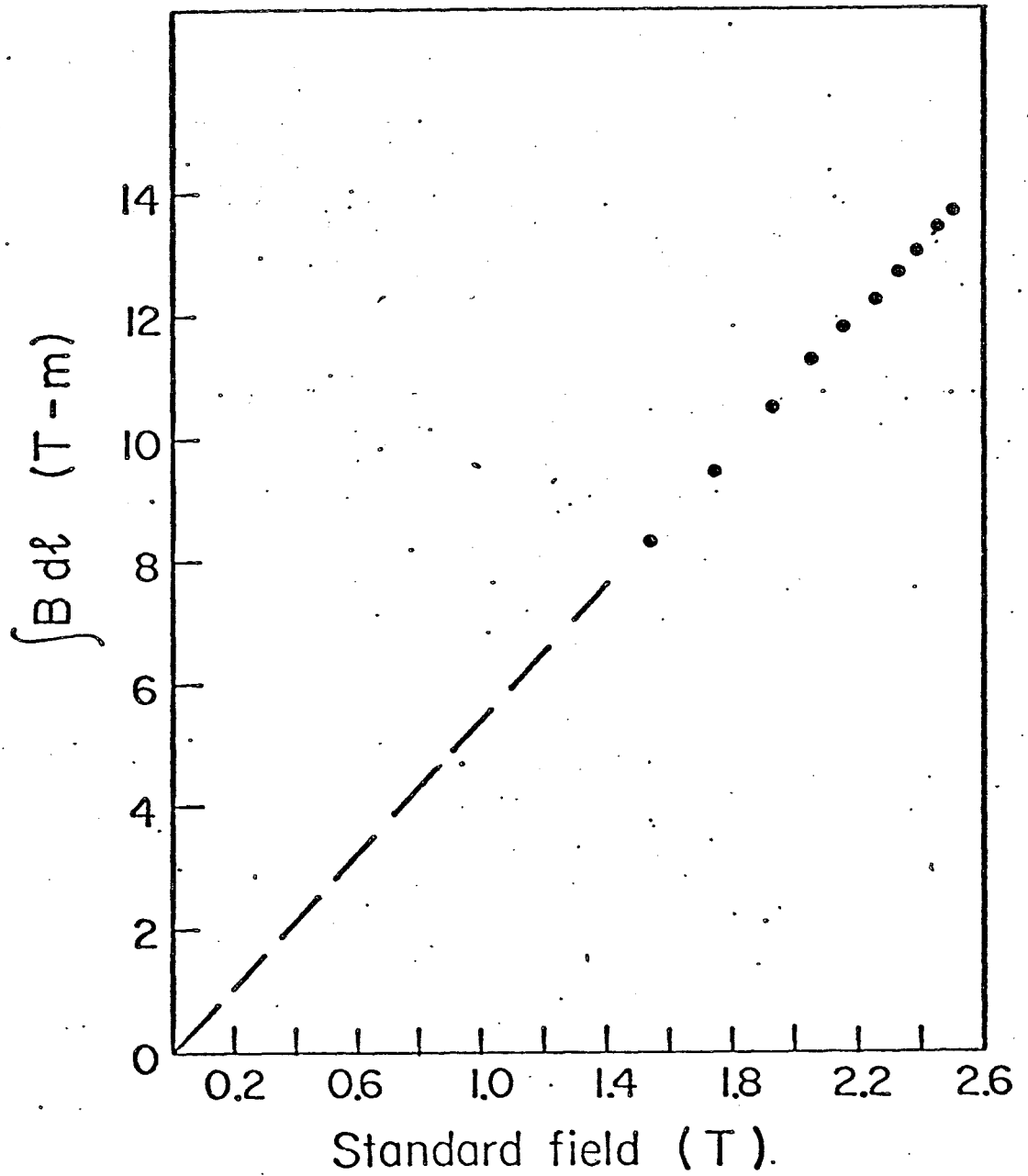


Figure 2.6 The field integral vs. the standard field.

Other possible sources of error, all negligible, were considered. The production target is 15 cm long, and the field integral over the target is 0.15% of the total field integral. If the production distribution of Λ^0 's is flat over the target length, then the rms deviation in field integral due to variation in production position is 0.04%. The Λ^0 decay vertices ranged over 11 meters, but the field integral over the decay region was 0.04% of the total.

The NMR probe in the standard position in the collimator was in place during all the field integral measurements. A given magnetic field at this point defined a set point for a particular field integral as measured by either the stretched wire probe or the NMR and Hall probes. Three non-zero values of the field integral were chosen for data-taking, ± 13.64 T-m, ± 10.55 T-m, and ± 9.05 T-m, corresponding to standard fields of 2.495 T, 1.939 T, and 1.662 T. These field integrals were reproduced using the standard field for each data run. The variation in the standard field over a one hour data run were negligible. The standard field was recorded for each data run, and run-to-run fluctuations in the standard field setting were 0.1% at most.

2.5 THE SPECTROMETER

An elevation view of the apparatus is shown in figure 2.2. Two meters downstream of the neutral beam collimator was a veto scintillation counter 10 cm in diameter followed by an 11 m long evacuated decay volume 36 cm in diameter. In this region the neutral beam was about 2 cm in diameter with 1 mrad total divergence. The trigger required nothing in the veto counter and at least one charged track in the first four proportional chambers downstream of the decay volume, and two charged tracks in the fifth chamber, one on either side. The momentum of each track was measured by bending the tracks in a magnetic field after the third proportional chamber. This magnet was a ferric superconductor whose aperture was 20.3 cm vertically by 61 cm horizontally and was 2.5 m long. The field integral was approximately 2.4 T-m, and was determined precisely by comparing the measured K_S^0 mass with its known value.

The proportional chambers were of conventional design and are described in detail elsewhere.¹⁹⁻²¹ The signal wire spacing was 2 mm and each chamber contained both a horizontal and a vertical signal plane except chamber 2 in which the wires were rotated through 45 degrees about the neutral beam axis. Chambers 1 and 3

had 256Vx128H wires, chamber 2 128x128 wires, chamber 4 316Vx128H wires, chambers 5 and 6 had 640Vx192H wires. The chambers were operated on a gas mixture of 70% Argon, 30% Isobutane, and 0.3% Freon bubbled through Methylal at 4°C. The operating voltage was 4.2 kV. In the spaces between the first five chambers were plastic bags filled with Helium to reduce multiple scattering.

2.6 TRIGGER LOGIC

Fast signals from the chamber planes were used in the trigger along with signals from the scintillators. Each chamber generated a fast pulse which was formed as a combination of a logical "OR" of the vertical wires and an "OR" of the horizontal wires. In chamber 5 the vertical wires were "OR"-ed in two parts, those wires to the left of the chamber center and those to the right each generating a fast "OR" pulse. The trigger logic is shown in figure 2.7. The trigger requirement was: no charged particle in the veto V, at least one charged particle in each of the first four chambers, at least one charged particle in the left side of chamber 5 and one in the right side of chamber 5, and at least one charged particle in TS, the scintillator behind chamber 1.

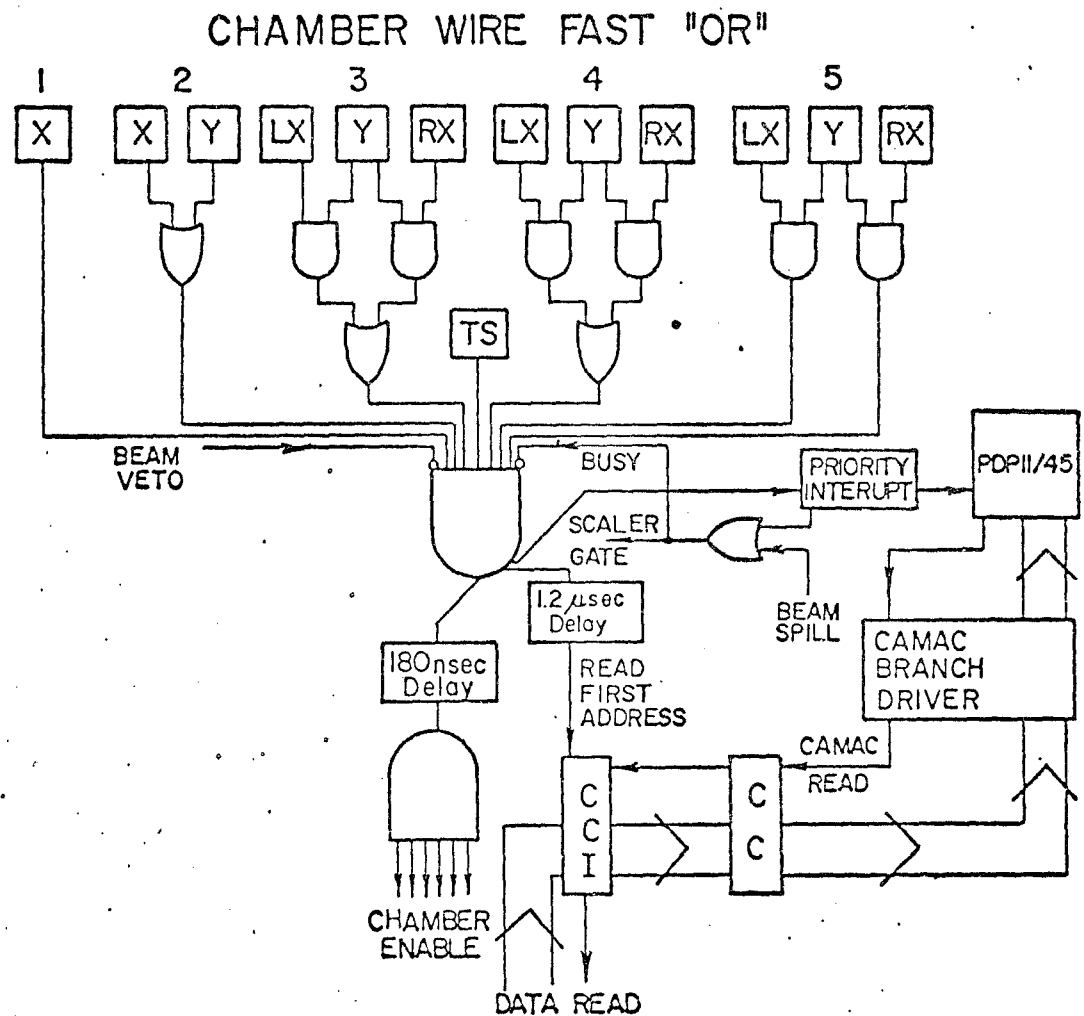


Figure 2.7 The electronic logic.

$$GE = \overline{V} \cdot TS \cdot CH1 \cdot CH2 \cdot CH3 \cdot CH4 \cdot CH5R \cdot CH5L$$

2.7 DATA ACQUISITION

If the trigger was satisfied, an enable pulse was sent to each chamber which caused flip-flops to be set, and stored the wire hit information for that event. The trigger logic also generated a busy logic level which prevented any further triggers from occurring during the chamber read-out process. A priority interrupt was sent to the PDP 11/45 computer, which caused the computer to read the chamber hit information serially via CAMAC. Reading the event caused all the chamber flip-flops to be reset. When this was finished, typically 0.5 msec later, the computer signalled its readiness for a new event.

At the end of each 2 sec beam spill the computer also read through CAMAC a set of 20 scalers which contained data from various beam monitors. The ion chamber data was also recorded and cleared at this time.

Events were read by the PDP 11/45 into core memory until a buffer was filled, at which time the buffer was transferred to disk. Three buffers could be held in core and, since the rate at which events could be written to

core exceeded the rate at which they could be transferred from core to disk, when core was filled data taking was halted to transfer this data to disk. The core-disk transfer time (the bulk of the dead-time) limited the number of events which could be collected during a spill to 880. At the end of a spill, the incomplete buffer in core was transferred to disk and the information on disk was written to tape. The events in the incomplete buffer were used to generate various histograms which served as valuable on-line diagnostics. A special scaler record was written at the end of each spill.

2.8 DATA TAKING CONDITIONS

Data were taken, half at +7.2 mrad, half at -7.2 mrad with an incident proton beam intensity of 2×10^8 protons per pulse. Approximately 880 triggers per spill were written to data tape, and at this rate a data tape was written every hour which contained 160000 triggers. Of these triggers about 50000 were Λ^0 's after all software cuts. So in 60 hours of data taking, 3×10^6 Λ^0 's were collected at 7.2 mrad. Several tapes were taken at 0 and 5 mrad as experimental checks. Table 2.1 shows the breakdown of tapes by production angle, spectrometer magnet polarity, and field integral.

In addition to those listed in the table, five tapes were taken with the production target out, one each at ± 7.2 mrad, ± 5 mrad, and 0 mrad for $\int B dl = +13.64$ T-m. Several tapes were taken with the collimator and production target out, for several sweeper field integrals, and with the production target bending magnets on to check the directions of the fields in these magnets by bending the proton beam and recording the wire chamber coordinates. A total of 86 data tapes was written.

θ SPEC		FIELD INTEGRAL (T-m)						
POL		13.64	10.55	9.05	0.00	-9.05	-10.55	-13.64
+7.2	+	4	2	2	1	2	2	4
	-	4	2	2	1	2	2	4
-7.2	+	4	2	2	1	2	2	4
	-	4	2	2	1	2	2	4
+5.0	+	1	0	0	0	0	0	0
	-	0	0	0	0	0	0	0
-5.0	+	0	0	0	0	0	0	0
	-	1	0	0	0	0	0	0
0.0	+	2	0	0	0	0	0	2
	-	2	0	0	0	0	0	2

Table 2.1 The distribution of data tapes written

CHAPTER 3

DATA ANALYSIS

The polarization of the Λ^0 sample was precessed in the sweeping magnetic field to obtain the magnetic moment. The angle through which the polarization precessed was

$$\theta = \frac{\mu_{\Lambda} c}{\hbar \beta} \int B dl$$

where $\beta = p/E$ was 1 to 0.02% or better, $\int B dl$ is the field integral in the sweeping magnet, and μ_{Λ} is the Λ^0 magnetic moment. The precession angle was measured for seven different precession fields and μ_{Λ} was calculated using the known values of $\int B dl$.

3.1 RECONSTRUCTION PROGRAM AND DATA SUMMARY TAPES

The analysis of each data tape was done in three parts. First the wire hit data was read from the data tape, decoded, and used to search for and reconstruct events of neutral vee topology. The momenta and vertex information for those events with acceptable vees was then written to a compacted data summary tape. This tape was read by a polarization analysis program which selected events with the Λ^0 mass and measured the decay asymmetry in the Λ^0 center of mass, yielding the polarization. A short tape was written by this program which allowed several data runs to be combined in a final magnetic moment analysis.

Each data tape contained the wire hit information for 160000 triggers and the scaler records for each spill. The wire hits were processed by a reconstruction program which searched for events of neutral vee topology. These were defined as events in which 1) the two charged tracks upstream of the spectrometer magnet intersected in the decay volume, 2) x- and y-views for each track correlated through chamber 2 (whose wires were rotated through 45 degrees), and 3) the track segments upstream and downstream of the spectrometer magnet intersected approximately halfway through the magnet.

For a production angle of 7.2 mrad, a typical data tape was 68% neutral vees, 22% events with no opening angle before the spectrometer magnet, and 10% events which failed to reconstruct.

For those events which were neutral vees, the slopes of both tracks and the vertex position were fitted, and the momentum of each track was calculated using a nominal field integral for the spectrometer magnet of 0.7266 Gev/c. All events which satisfied the neutral vee criteria were written to a compacted data summary tape, along with scaler records. For each event the vertex position, the momentum components of each of the two charged tracks, and the error matrix for the fit of the tracks to a vee were written to the data summary tape.

3.2 EVENT SELECTION

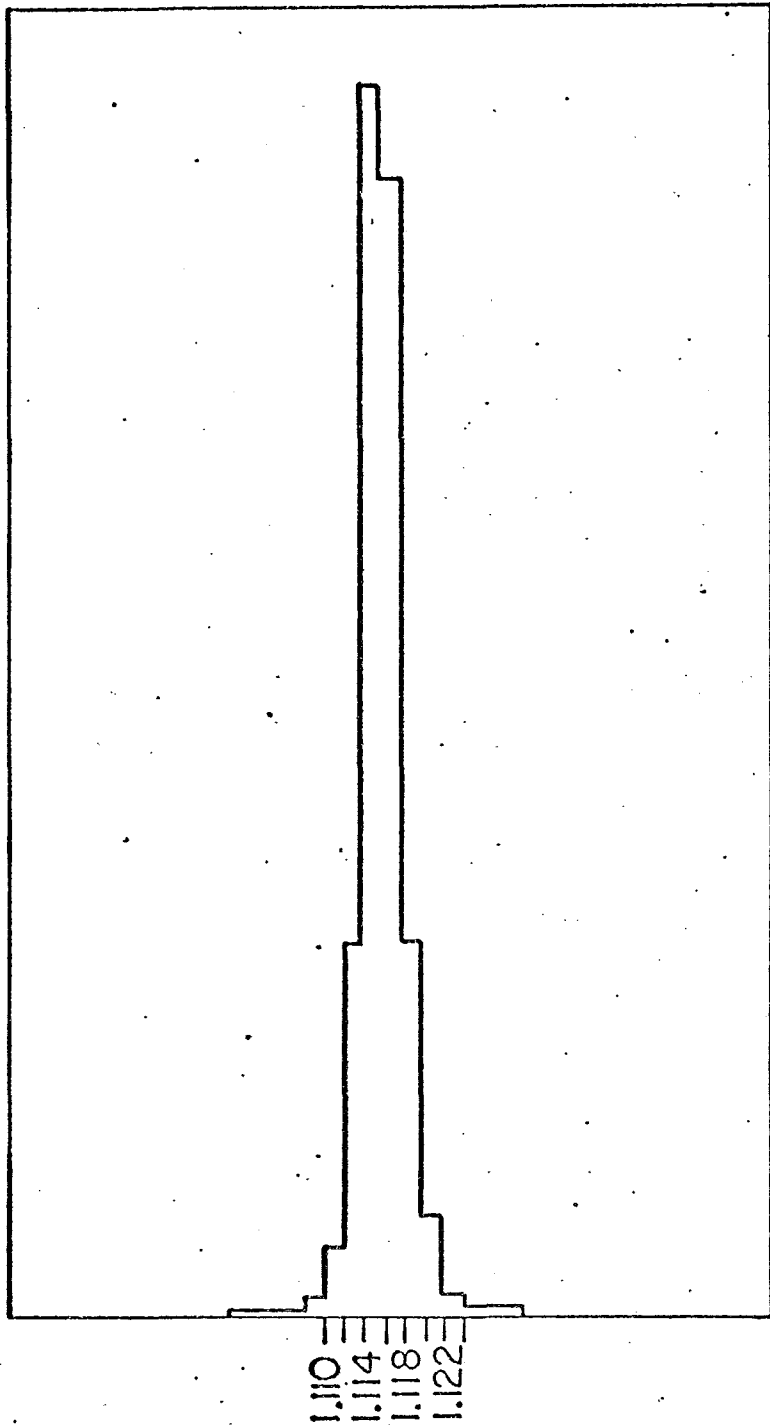
This compacted tape was processed by a program which made several cuts on the neutral vees. First the momenta were recalculated using the spectrometer magnetic field integral corrected to yield the proper mass for K_S^0 events. For events where the positive track had the higher momentum the invariant mass was calculated assuming that the positive track was a proton and the

negative track a pion. If the mass fell within 3σ (σ = mass measurement error as calculated from the error matrix for the vee fit) of the known Λ^0 mass (1.1156 Gev/c²) the event was accepted as a Λ^0 . The invariant mass of the Λ^0 sample is shown in figure 3.1. The full width at half maximum is 4 Mev/c². The K_S^0 contamination of this sample was approximately 0.5%. The momentum spectrum of this Λ^0 sample for a production angle of 7.2 mrad is shown in figure 3.2.

Forty-three percent of the triggers and 64% of the reconstructed neutral vees were Λ^0 's at 7.2 mrad. Twenty-seven percent of the neutral vees were K_S^0 's, 4% were $\bar{\Lambda}^0$'s, and 5% had neither mass. The acceptance for neutral vees of known mass is shown in figure 3.3. Above a momentum of 150 Gev/c most decays in the decay volume were accepted. Below this, the geometric acceptance of the spectrometer falls rapidly with momentum.

A study of the yield of Λ^0 's per incident proton showed that the positive production angle was larger than the negative production angle (in absolute value) by approximately 0.5 mrad at the nominal 7.2 mrad setting. As will be seen in Section 3.4, this does not affect the result.

RELATIVE NUMBER OF EVENTS



p-π INVARIANT MASS
(GeV/c²)

Figure 3.1 The p-π invariant mass.

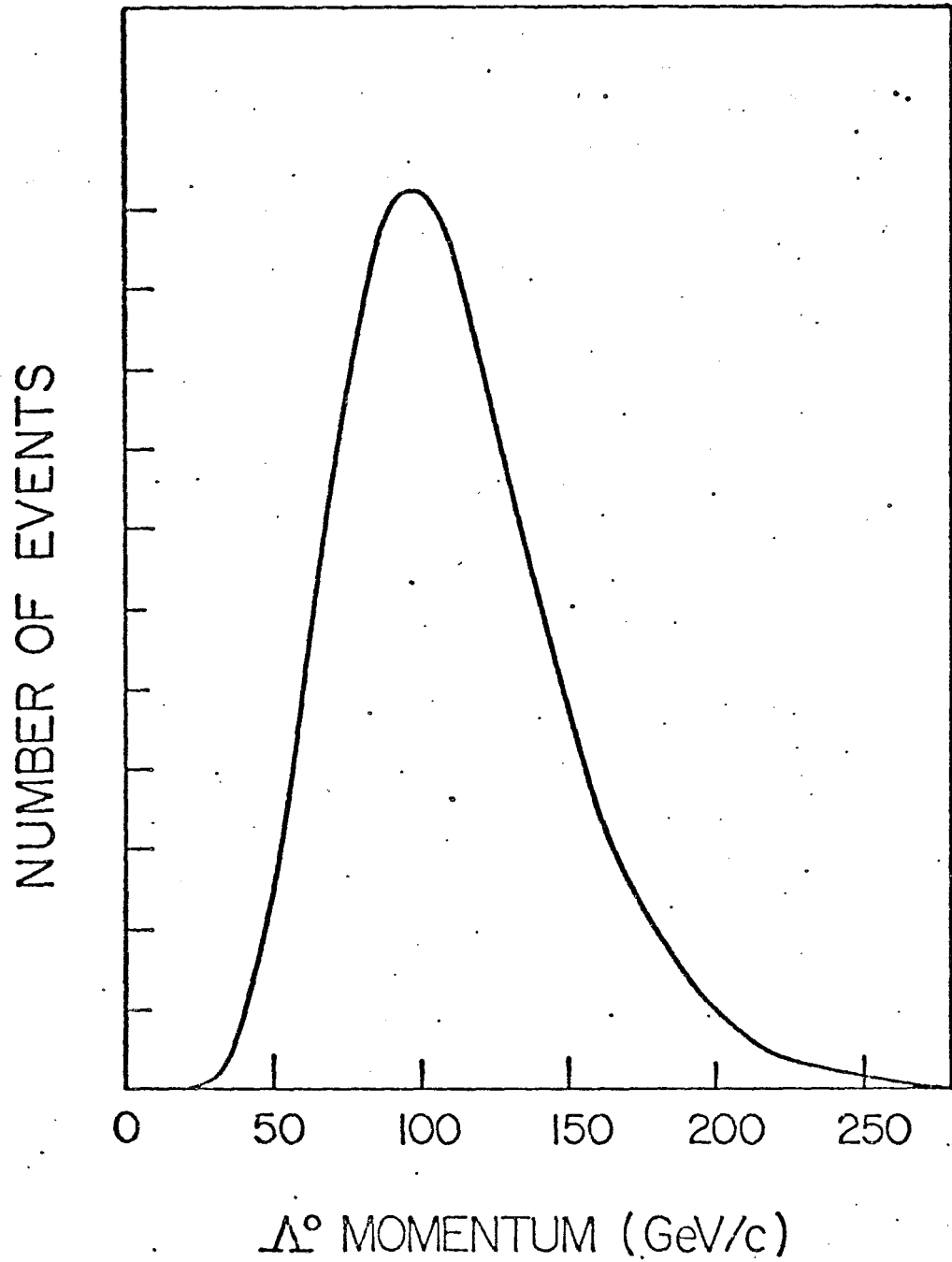


Figure 3.2 The Λ^0 momentum spectrum.

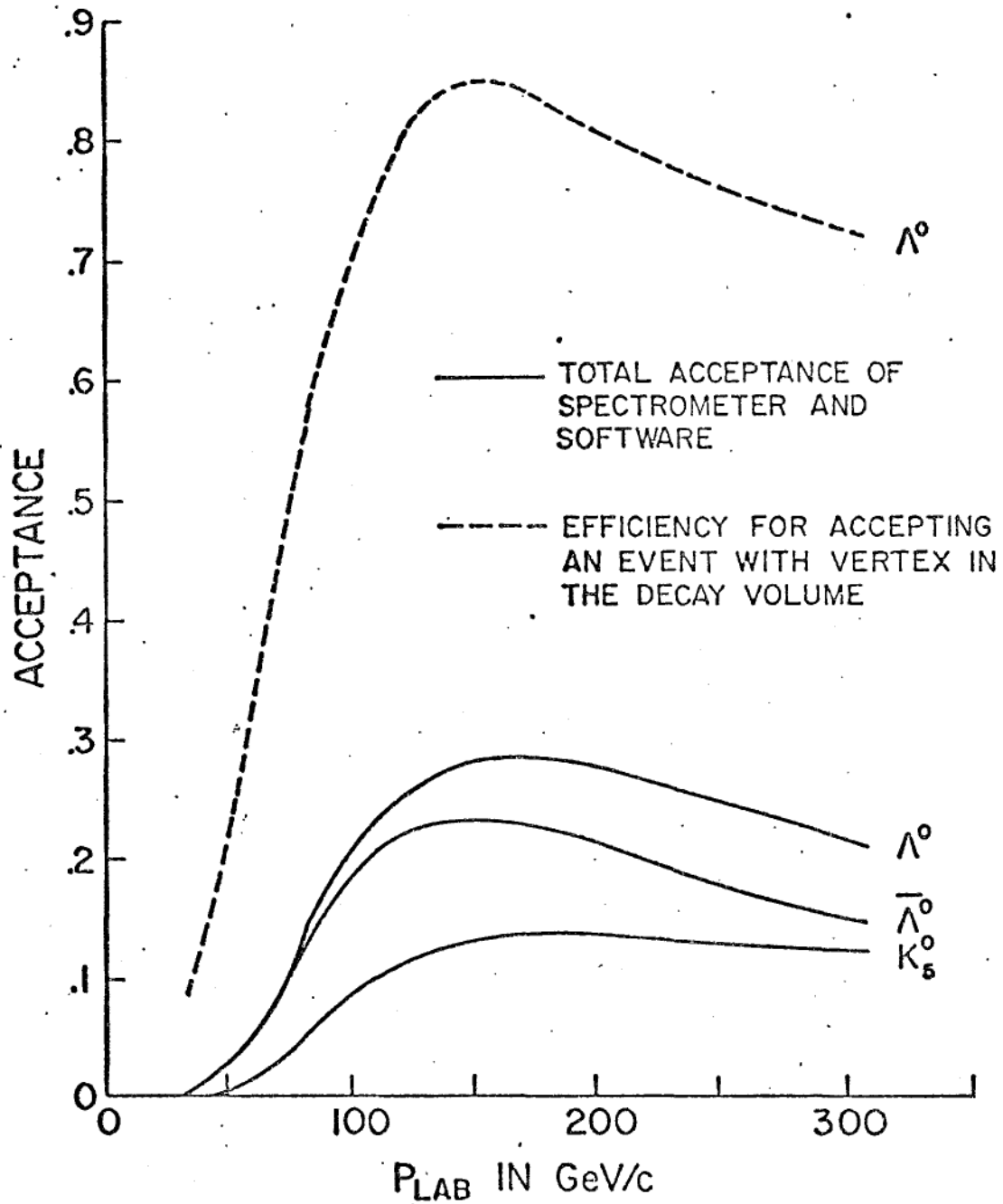


Figure 3.3 The acceptance for Λ^0 , $\bar{\Lambda}^0$, and K_S^0 as a function of momentum.

The vertex position of Λ^0 's was then required to be inside the decay volume within errors. Figure 3.4 shows the distribution of decay vertices. The veto was at 207 cm, and the first chamber at 1300 cm.

The Λ^0 momentum vector was used to extrapolate back to the production target, and each event was required to point within $R^2=40 \text{ mm}^2$ of the target center. The R^2 distribution is shown in figure 3.5. This cut served to reduce two sources of background. Approximately half of the Λ^0 's produced in the collimator (approximately 5% of the total) and approximately 90% of the Λ^0 's from Ξ^0 decay (Ξ^0 events constitute only 1% of the triggers for all R^2) were eliminated by this cut.

The angle in the yz plane of the Λ^0 with respect to the neutral beam direction is shown in figure 3.6. The secondary peak for positive production angle is due to Λ^0 's produced in the beam focus scintillators 1.22 meters upstream of the target. Events with $-1.25 > \theta_y > 1.50$ mrad were cut, to eliminate this secondary source from the data sample.

A least squares fit was performed, with the measured pion and proton momenta as input data, constraining the event to have the Λ^0 mass. The fitted momenta were used in the remaining analysis.

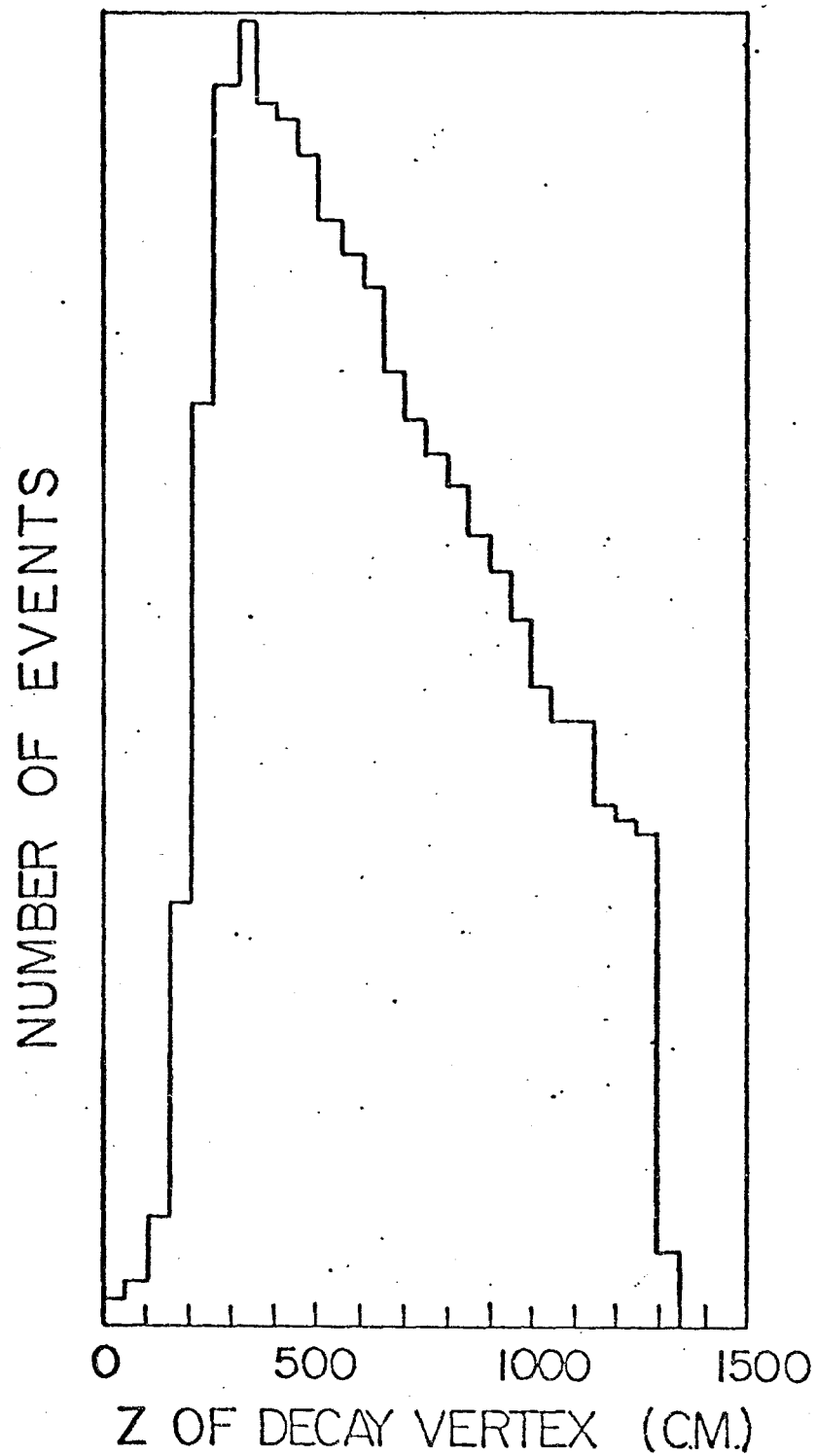


Figure 3.4 The Λ^0 decay vertex distribution.

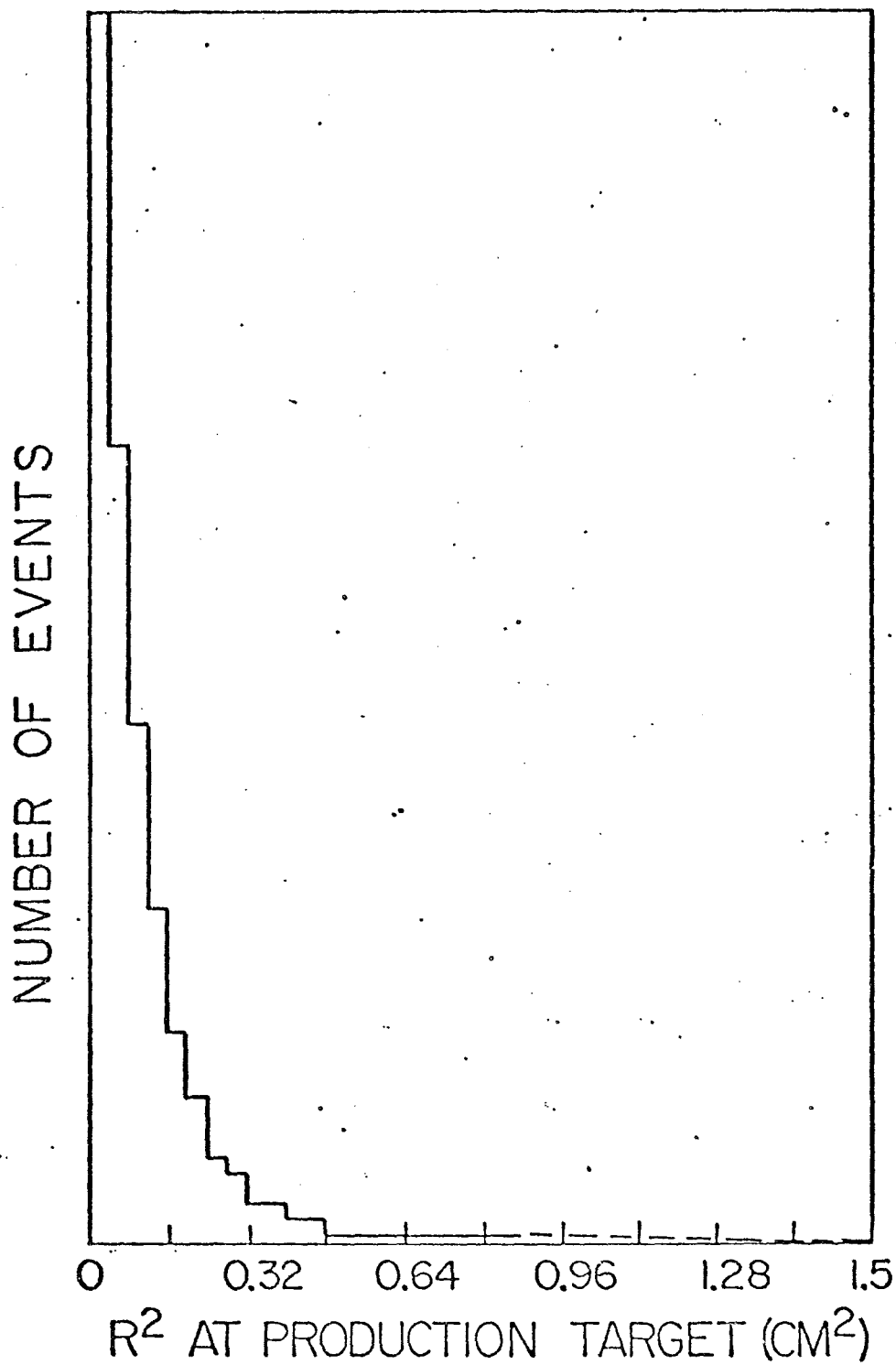


Figure 3.5 R² at the production target.

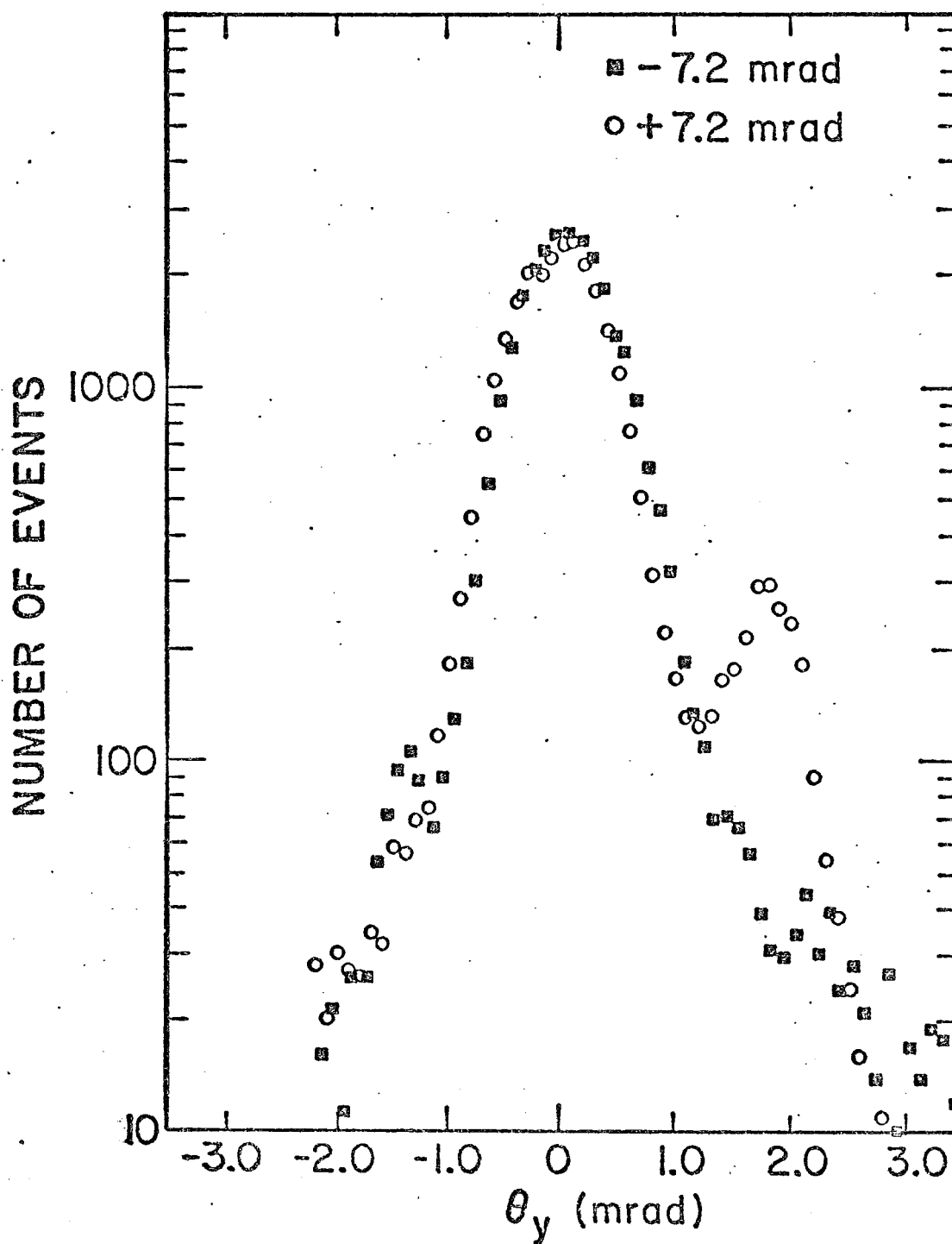


Figure 3.6 The angle with respect to the z axis in the y-z plane for Λ^0 's.

The fitted tracks for each event were required to pass several geometric cuts designed to mock the experimental apertures. These cuts were slightly more restrictive than the real apertures. Events which passed all tests were used in the polarization analysis.

3.3 THE POLARIZATION ANALYSIS

The polarization was determined through the asymmetry in the Λ^0 rest frame. The proton angular distribution in the Λ^0 rest frame for a sample of Λ^0 's is

$$dN(\hat{p}_p) = \frac{1}{2} (1 + \alpha \vec{P}_\Lambda \cdot \hat{p}_p) d \cos \theta^*$$

where $\alpha = -0.647 \pm 0.013^{22}$, \hat{p}_p is the proton direction in the Λ^0 rest frame, \vec{P}_Λ is the polarization of the Λ^0 sample and $\cos \theta^* = \vec{P}_\Lambda \cdot \hat{p}_p$. In this analysis three fixed directions in space $(\hat{x}, \hat{y}, \hat{z})$ were chosen, the $\cos \theta^*$ distribution was obtained for $\cos \theta^* = \hat{p}_p \cdot \hat{x}$, $\hat{p}_p \cdot \hat{y}$, $\hat{p}_p \cdot \hat{z}$ and the components of the polarization along these directions were calculated. The direction of the polarization then yielded the precession angle and the magnetic moment for each momentum bin.

The distribution of events in $\cos \theta^*$ was distorted by the acceptance of the spectrometer, and it was not possible to determine the polarization by a simple linear fit to the raw distributions. Instead, a sample of Monte Carlo events were generated which reflected the spectrometer acceptance, and which were weighted by a polarization parameter $\propto P_{MC}$. This parameter was varied by χ^2 techniques until the two distributions agreed.

Two requirements must be met by the Monte Carlo distribution. First, it must be identical to the distribution of real events in all parameters except $\cos \theta^*$. Second, acceptance criteria for the two samples should be as similar as possible.

For each real event, Monte Carlo events were generated varying only $\cos \theta^*$, leaving the other event parameters unchanged. Thus the Monte Carlo events had the same vertex and momentum distributions as the real events. These Monte Carlo events were required to pass the same geometric cuts as the real events, and Monte Carlo events were generated until 10 passed these cuts. The distribution of real and Monte Carlo events at each of the geometric apertures used to define the acceptance were also compared in order to test for differences between the two samples. The χ^2 per degree of freedom

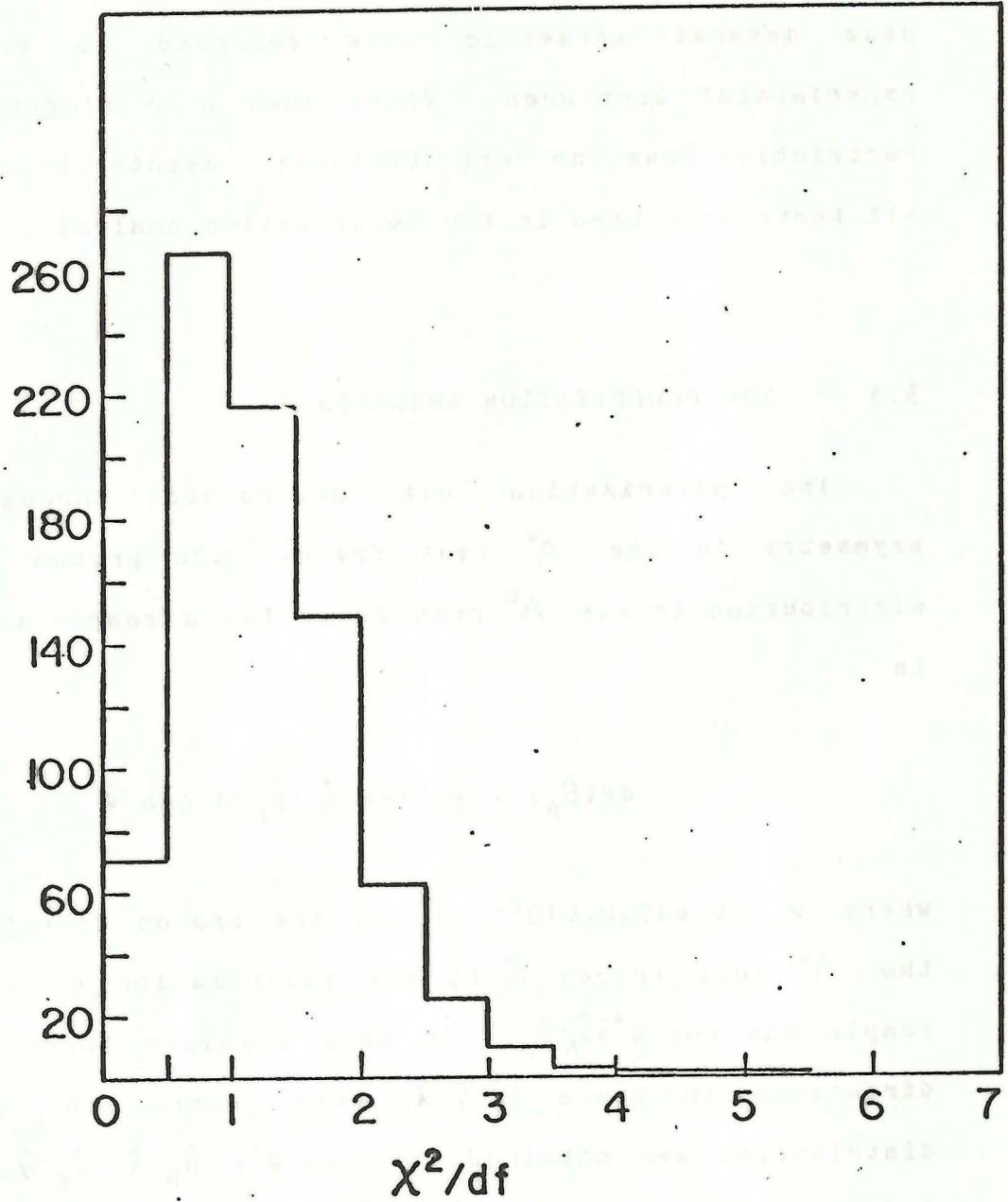


Figure 3.7 χ^2 per degree of freedom for fits of Monte Carlo geometric distributions to real event distributions.

distribution for these fits is shown in figure 3.7.

The distribution of real events reflects any real polarization, αP_R , which exists in the data. Since the Monte Carlo events are based on this distribution, they will also reflect the real polarization. The Monte Carlo distribution must be corrected for this. Each Monte Carlo event generated was weighted by

$$W = \frac{1 + (\alpha P_\Lambda)_{MC} \cos \theta_{MC}^*}{1 + (\alpha P_\Lambda)_R \cos \theta_R^*} \quad 1$$

where θ_R^* (θ_{MC}^*) refers to the real (Monte Carlo) event. The numerator polarized the $\cos \theta_{MC}^*$ distribution by the parameter $(\alpha P_\Lambda)_{MC}$. The denominator corrected this distribution for possible polarization in the real events. The value of $(\alpha P_\Lambda)_R$ was unknown, but the fit should result in $(\alpha P_\Lambda)_{MC} \approx (\alpha P_\Lambda)_R$. Therefore this equality was assumed throughout the calculation.

The weight was written as an expansion

$$W = 1 + \sum_I (-\alpha P_\Lambda)^I (\cos \theta_R^*)^{I-1} (\cos \theta_R^* - \cos \theta_{MC}^*)$$

and only the first four terms in the expansion were kept.

A χ^2 was constructed

$$\chi^2 = \sum_J \frac{(N_R(J) - N_{MC}(J, \alpha P_\Lambda))^2}{N_R(J)}$$

where J was the bin in $\cos \theta^*$ (twenty bins were used), N_R was the number of real events and N_{MC} was the sum of the weights, w . N_{MC} was renormalized to satisfy

$$\sum_J N_{MC}(J) = \sum_J N_R(J)$$

χ^2 and its first and second derivatives with respect to αP_Λ were calculated and χ^2 was minimized, using Newton's method, to obtain αP_Λ . The value of χ^2 was an indication of the goodness-of-fit of the $\cos \theta_{MC}^*$ distribution to the $\cos \theta_R^*$ distribution. This polarization analysis was performed for seven momentum bins, 30 Gev/c wide, from 60 to 270 Gev/c. The data were also split into positive and negative 7.2 mrad production angles and positive and negative spectrometer field for each of the seven magnetic field integrals. The polarization components along x, y, and z were calculated for each of these bins. The distribution of χ^2 from these fits is shown in figure 3.8.

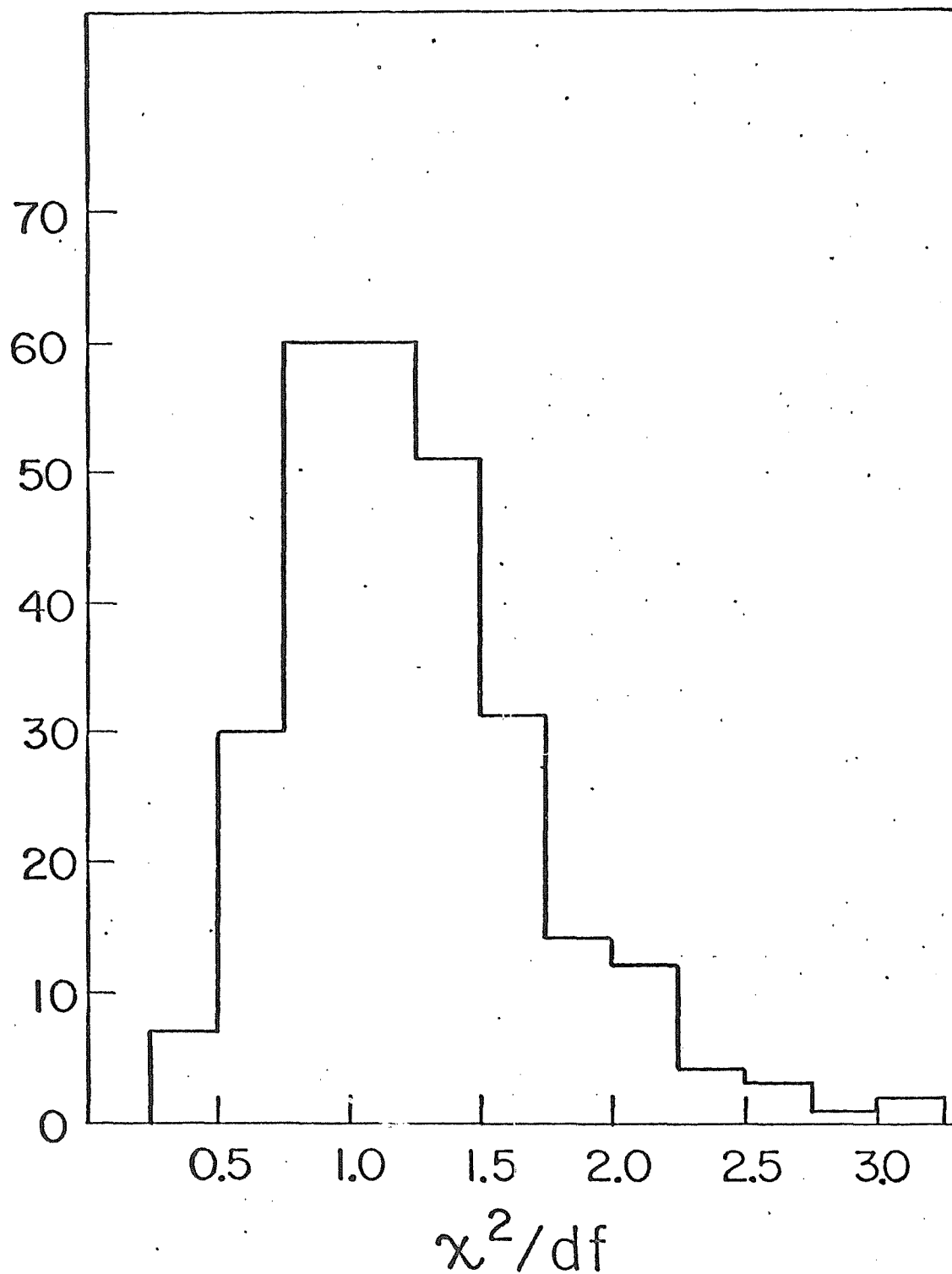


Figure 3.8 χ^2 per degree of freedom distribution for fits of Monte Carlo $\cos \theta^*$ distributions to real event $\cos \theta^*$ distributions.

These data could then be combined in several ways to calculate the magnetic moment.

3.4 POLARIZATION AND EXPERIMENTAL BIASES

The Λ^0 polarization at the production target was perpendicular to the production plane, in the parity allowed direction $-(\vec{k}_p \times \vec{k}_\Lambda)$ where \vec{k}_p (\vec{k}_Λ) is the incident proton (Λ^0) momentum direction. Positive polarization is defined along $\vec{k}_p \times \vec{k}_\Lambda$. The polarization is shown in figure 3.9 as a function of Λ^0 momentum. Since the incident proton beam and the outgoing Λ^0 direction defined a vertical plane (\vec{k}_Λ was in the horizontal plane within ± 1 mrad) the polarization at production was along $-\hat{x}$ ($+\hat{x}$) for positive (negative) production angles. The coordinate system and polarization direction are illustrated in figure 3.10. The magnetic field which precessed the polarization was along the $-\hat{y}$ direction for positive field integral, so the polarization precessed about the \hat{y} direction in the horizontal plane. The peculiar sign convention arose from previous experiments in this apparatus. When the production angle, θ , was reversed, the initial polarization direction reversed allowing cancellation of asymmetries due to the

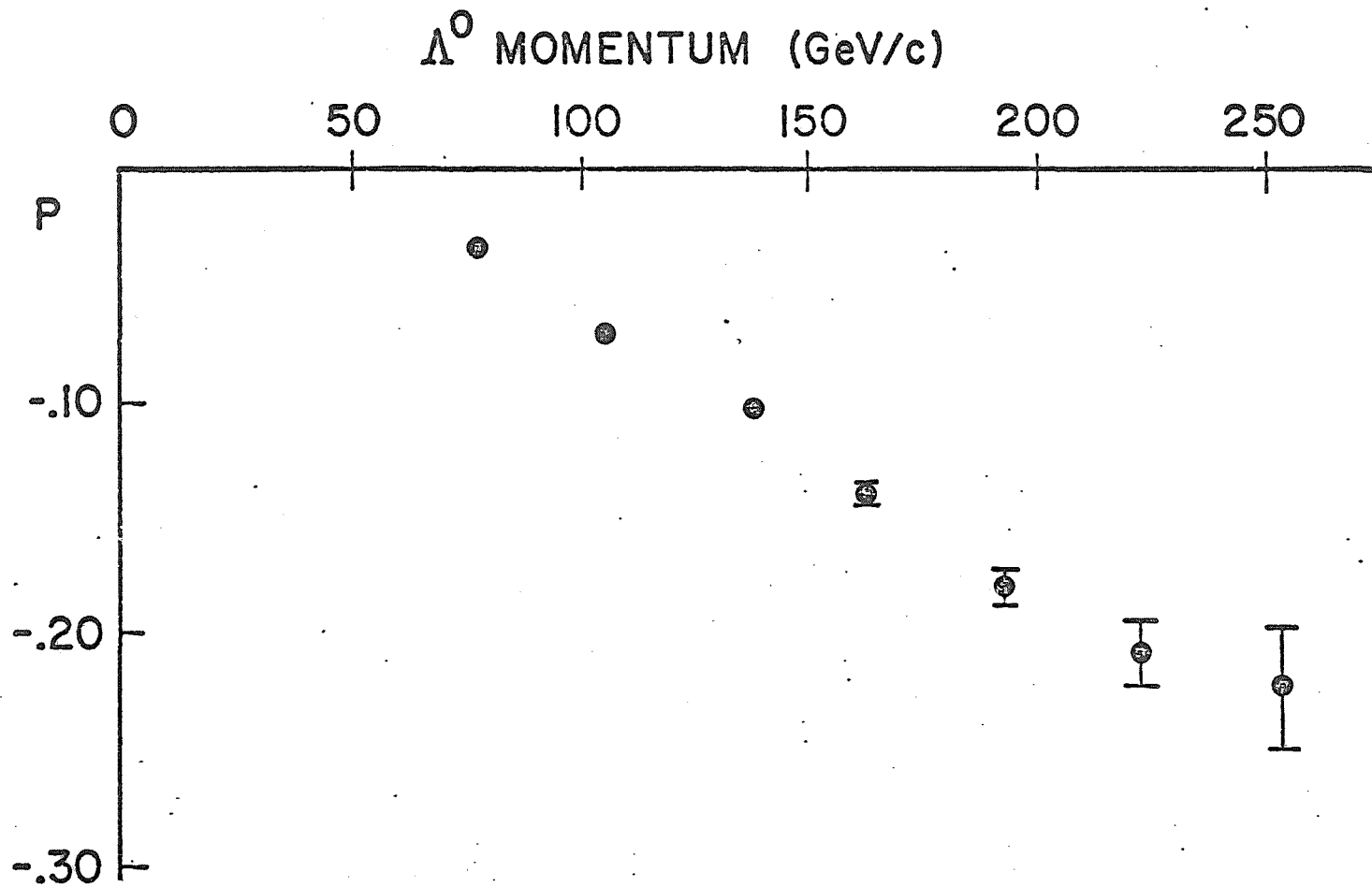


Figure 3.9 The Λ^0 polarization as a function of momentum.

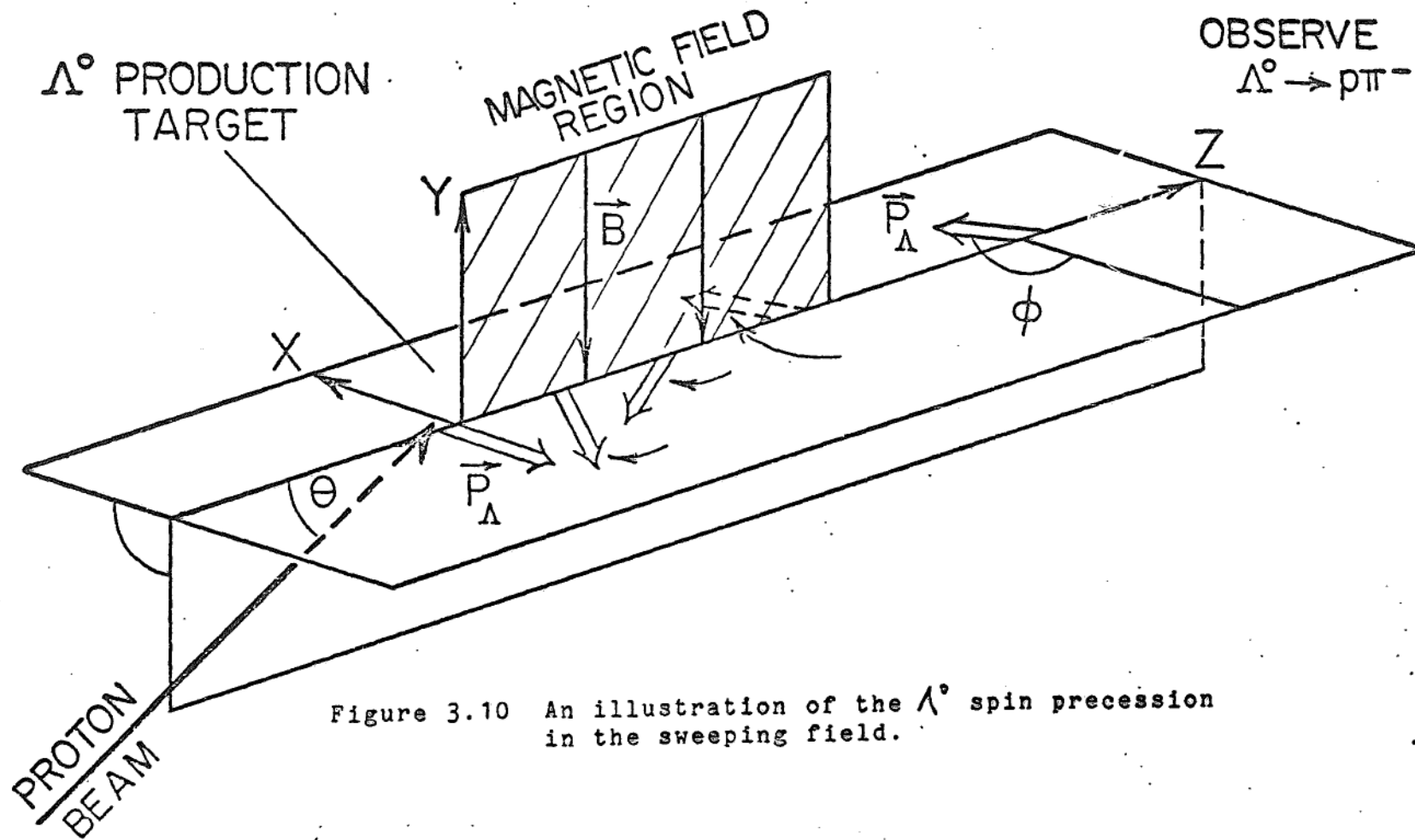


Figure 3.10 An illustration of the Λ° spin precession in the sweeping field.

acceptance of the spectrometer not accounted for in the Monte Carlo. Thus all components of the polarization were calculated

$$\alpha_P = \frac{\alpha_P(+\theta) - \alpha_P(-\theta)}{2} \quad 2$$

and the biases along each direction were

$$B = \frac{\alpha_P(+\theta) + \alpha_P(-\theta)}{2} \quad 3$$

The size of these biases is shown in figure 3.11 as a function of Λ° momentum.

The cancellation of biases was crucial to the precise determination of the magnetic moment. It was necessary that the biases be independent of production angle sign and magnitude. Several checks on the cancellation of biases were possible.

First, since the polarization at production was along $+\hat{x}$ and precessed through an angle between 90 and 180 degrees, the z component reversed when the field direction was reversed. This allowed an independent calculation of the bias in the z direction

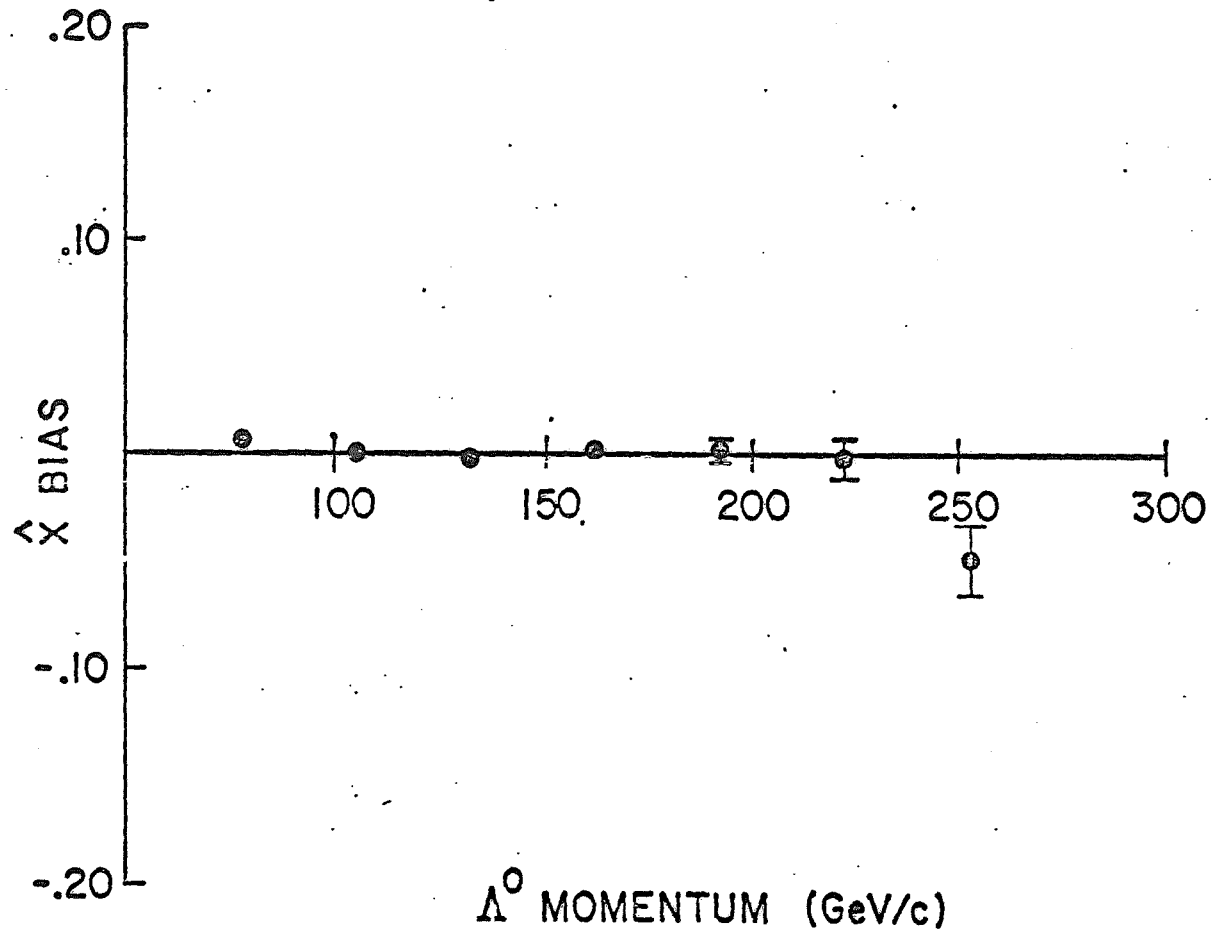


Figure 3.11a The x bias (B) versus momentum.

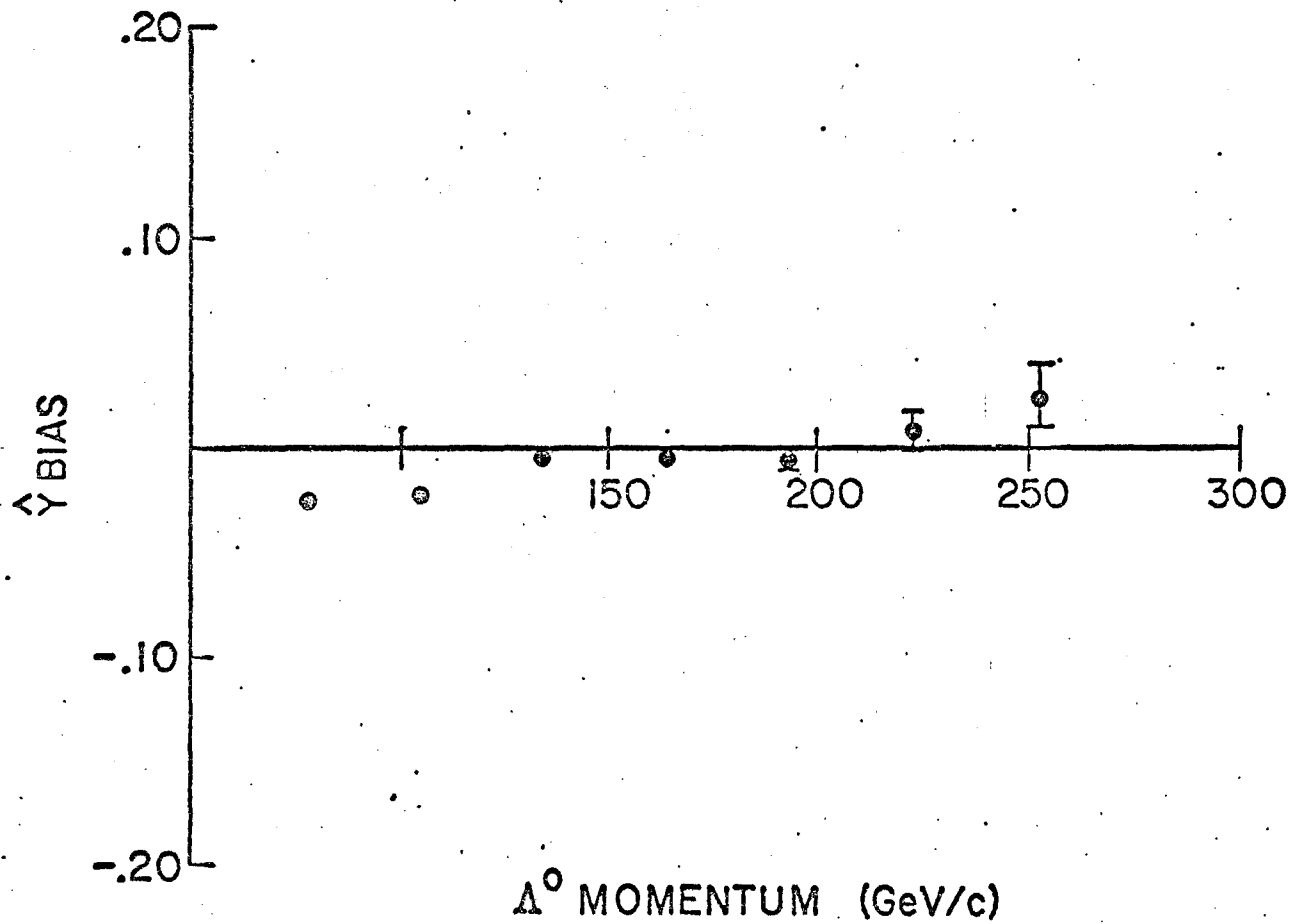


Figure 3.11b The y bias (B) versus momentum.

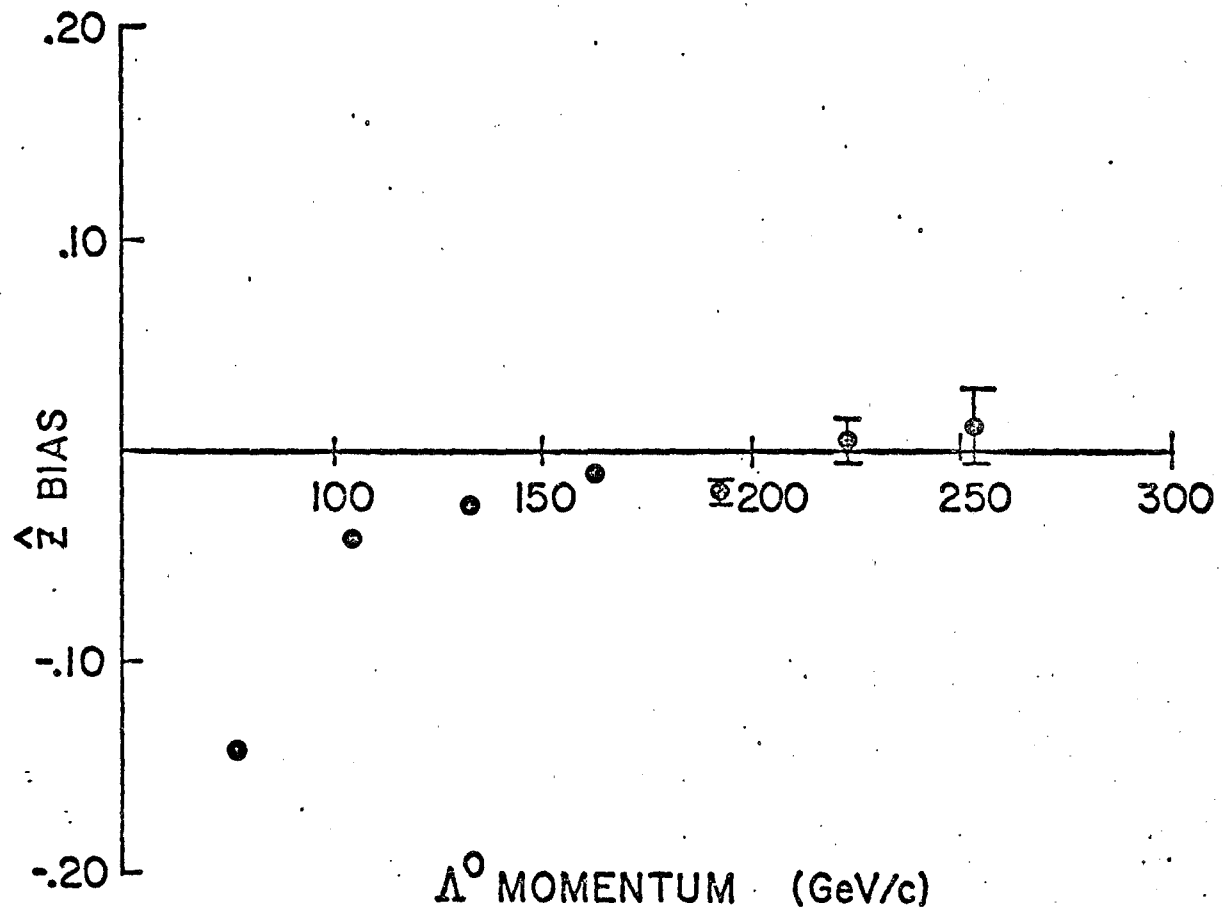


Figure 3.11c The z bias (B) versus momentum.

$$B_z = \frac{\alpha P_z(+ Bdl) + \alpha P_z(- Bdl)}{2}$$

4

for each production angle sign separately. Figure 3.12 shows a comparison of the z bias for positive and negative 7.2 mrad production angles calculated as in Eqn. 4 and the bias calculated as in Eqn. 3 for all field integrals.

Another check of bias cancellation is shown in figure 3.13. This figure shows the Λ^0 polarization for 0 mrad production angle. The z bias has been cancelled as in Eqn. 4. Since the z polarization at 0 mrad is zero as it must be by symmetry, the z biases have cancelled completely. The x and y biases could not be cancelled using the 0 mrad data alone, so figures 3.13a and 3.13b show the sum of the bias and the polarization. This sum for x is consistent with zero. Since the 7.2 mrad x bias is consistent with zero, and the biases are independent of production angle (figures 3.12 and 3.15), the x polarization is also zero at 0 mrad. The y polarization does not affect the magnetic moment measurement.

The polarization along the y direction is non-zero if parity is not conserved, or if the collimator axis and the incident proton beam axis (at finite production

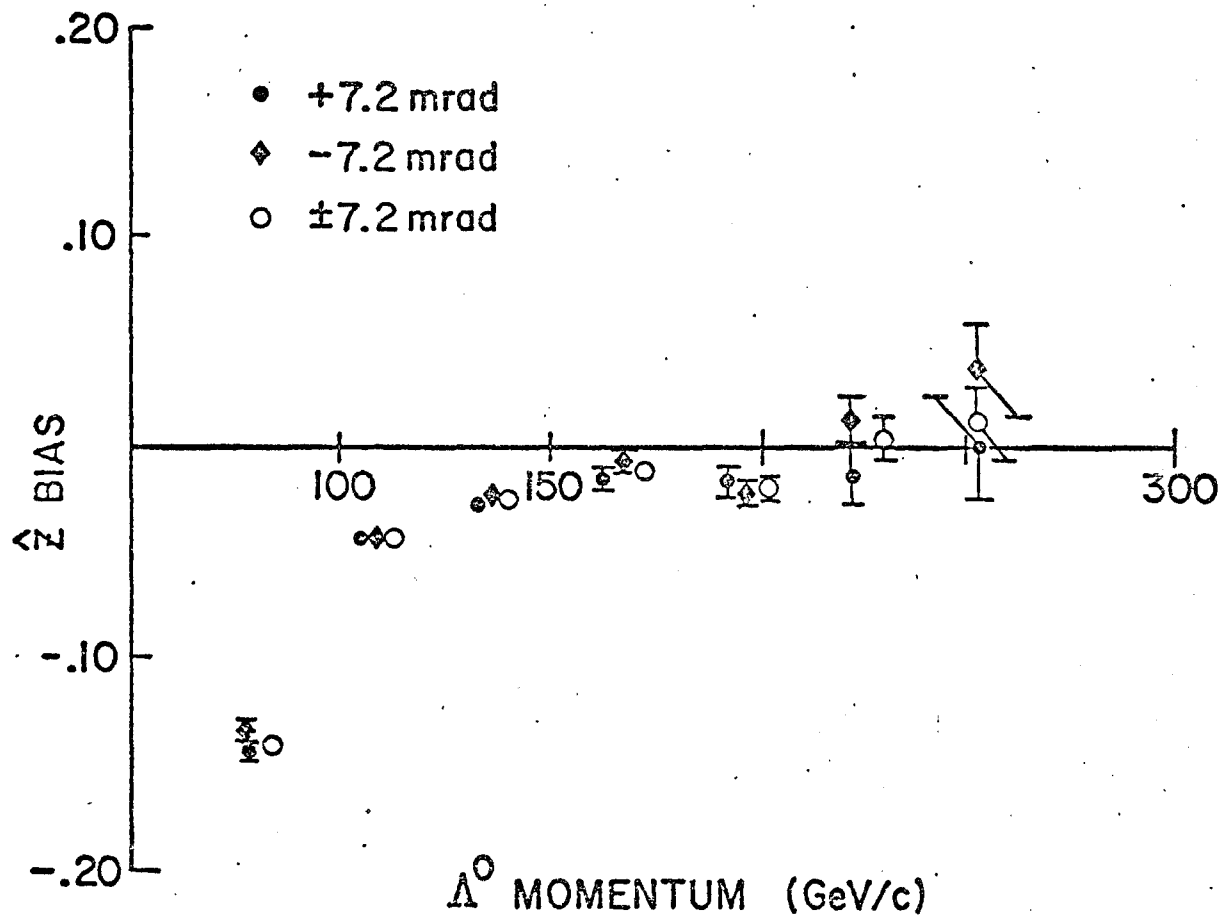


Figure 3.12 The z bias (B) versus momentum for both production angle signs separately.

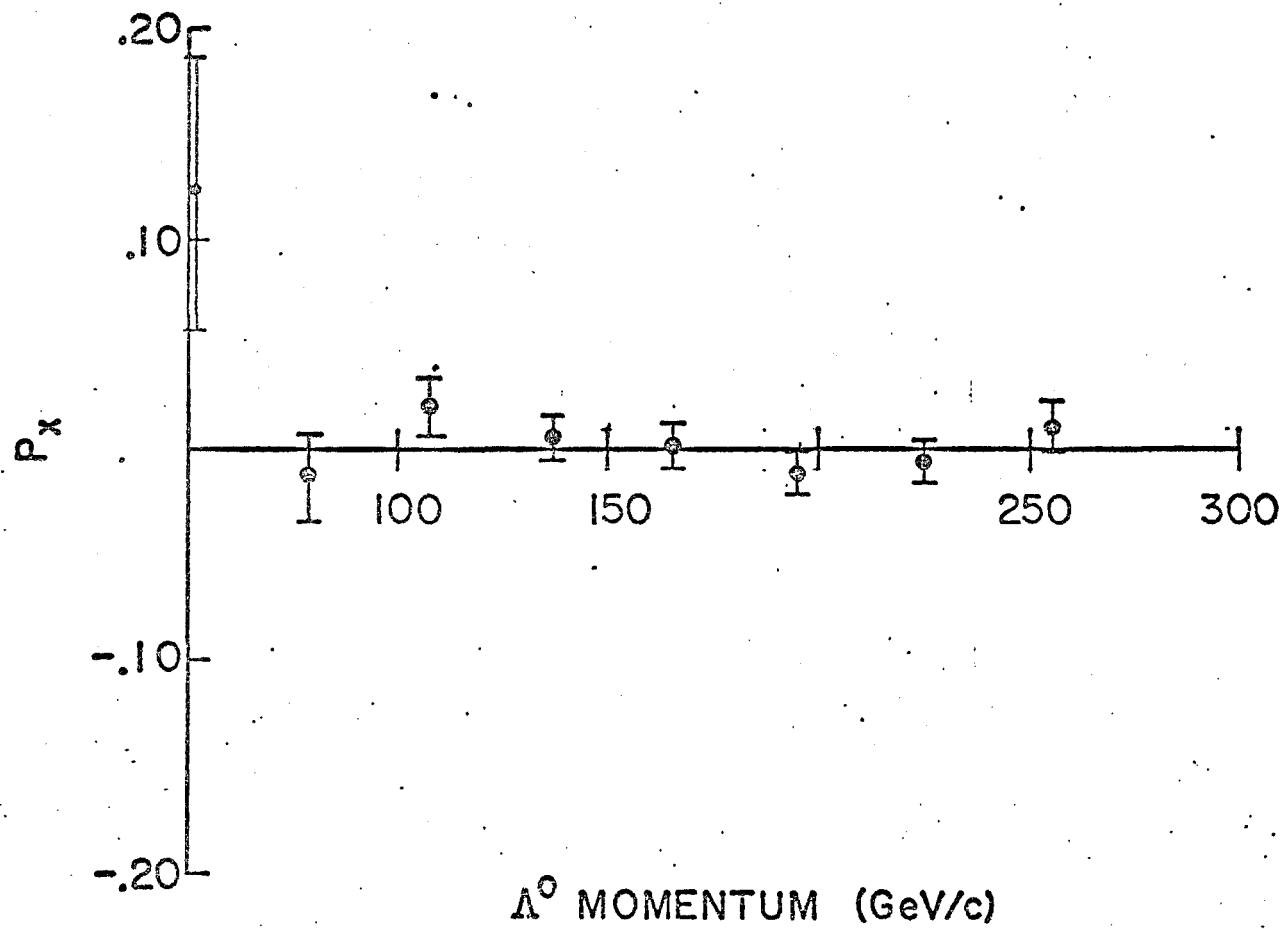


Figure 3.13a The $\times 0$ mrad polarization.

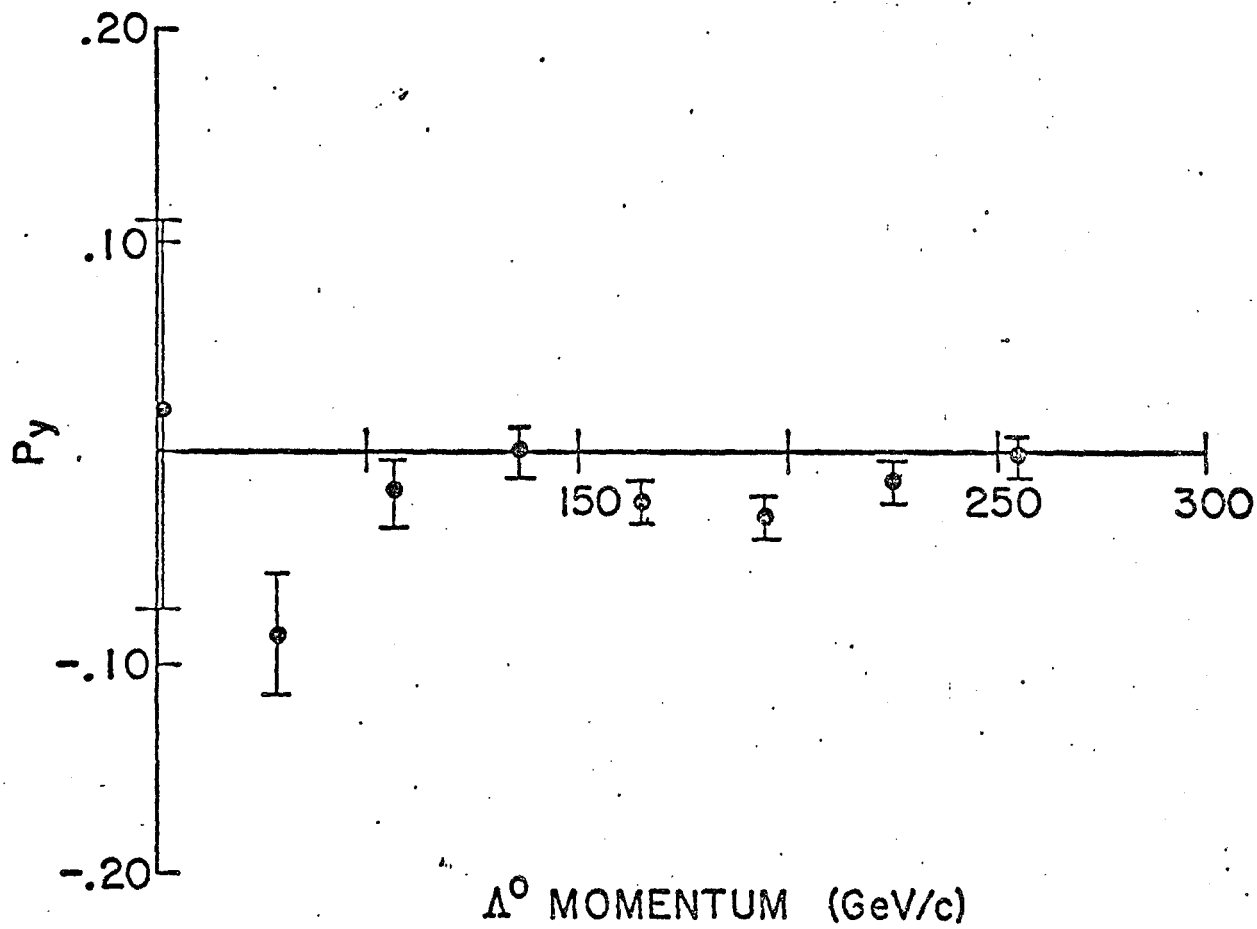


Figure 3.13b The y 0 mrad polarization.

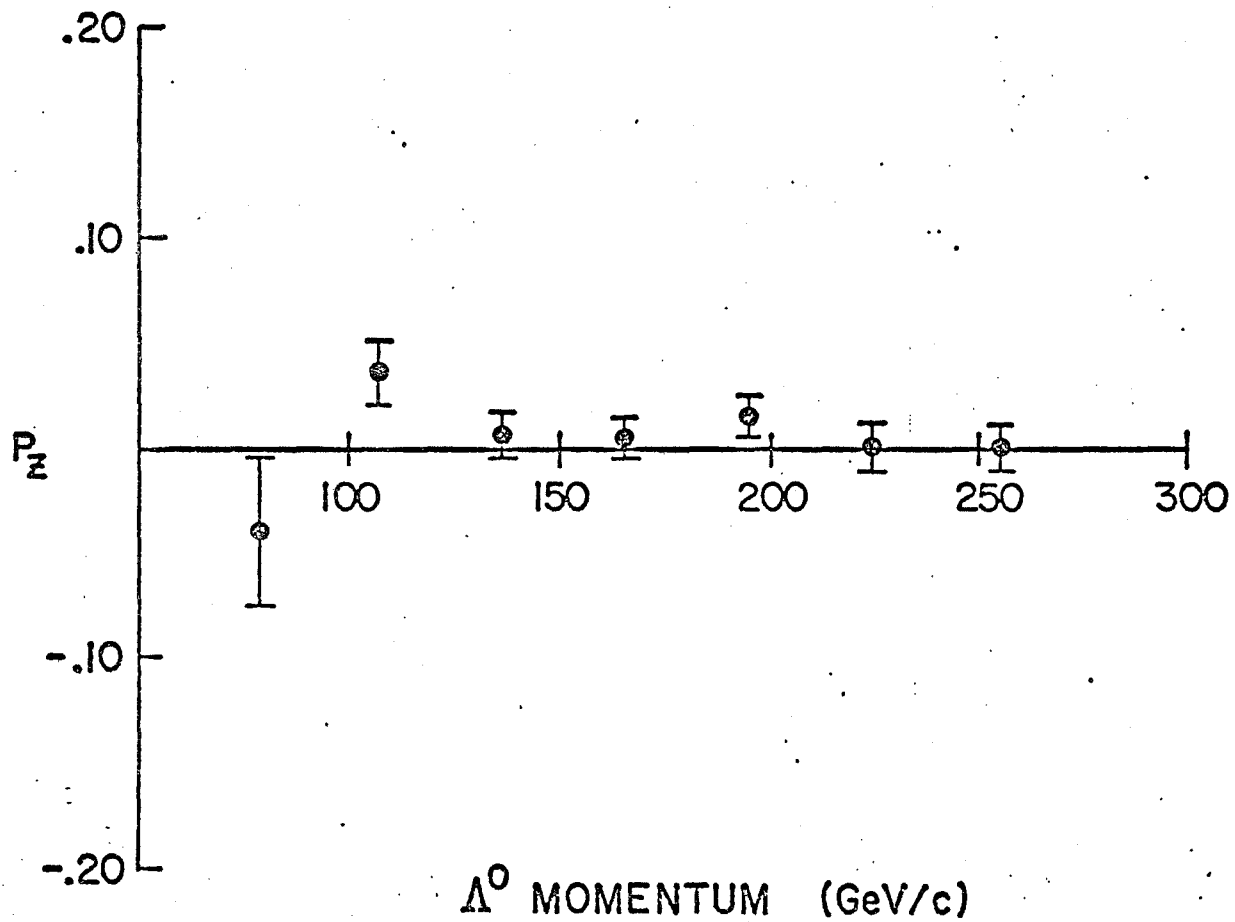


Figure 3.13c The z 0 mrad polarization.

angle) do not form a plane, or if the sweeping magnet field is not along \hat{y} . Figure 3.14 shows this polarization at 7.2 mrad, with the biases cancelled as in Eqn. 3. The y polarization is consistent with zero, which is evidence for parity conservation, proper alignment of the apparatus, and proper bias cancellation.

A comparison of the biases for several production angles is presented in figure 3.15. The 0 mrad z bias is calculated as in Eqn. 4. Since the biases are independent of production angle as shown in figures 3.12 and 3.15, the 0.5 mrad production angle difference (see Section 3.2) does not affect the magnetic moment measurement.

Since data were taken at several different field integrals, for both positive and negative production angles, the biases for each sweeper field could be calculated as in Eqn. 3. The results, displayed in figure 3.16, demonstrate that the biases are independent of field integral.

Two types of biases were present in the data. Both were independent of precession field and production angle, but depended on momentum. The first was the production angle bias, B, which has been described above.

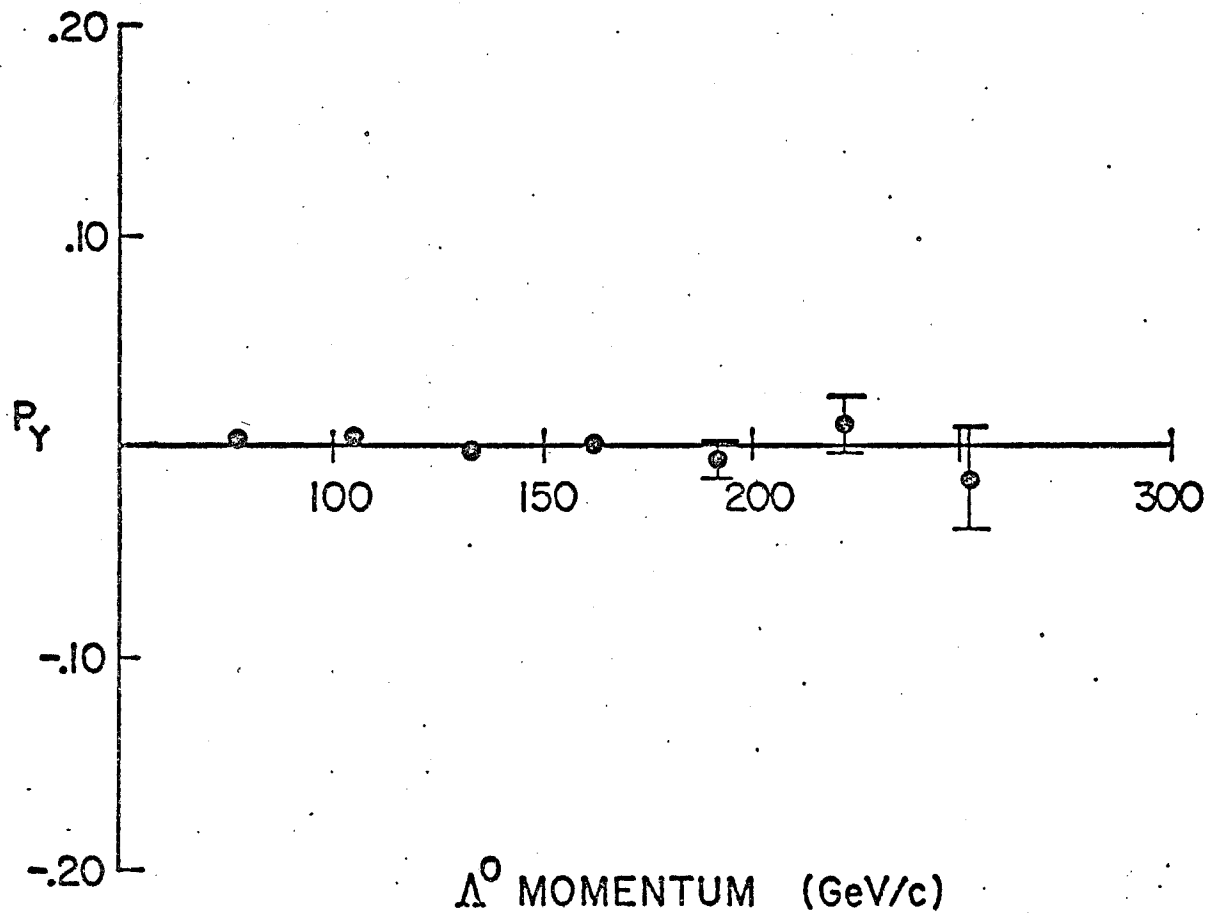


Figure 3.14 The 7.2 mrad y polarization.

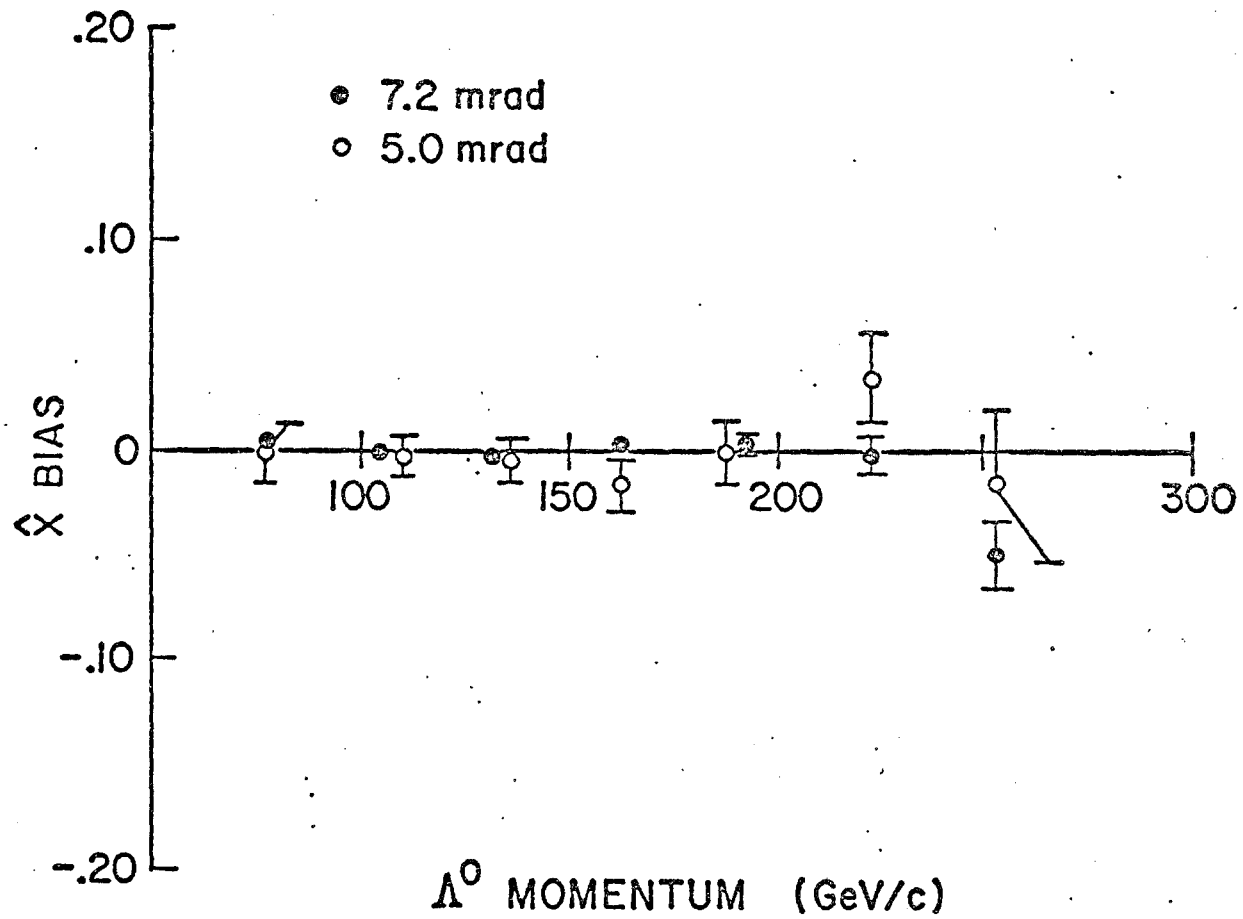


Figure 3.15a The x bias (B) for 5 and 7.2 mrad.

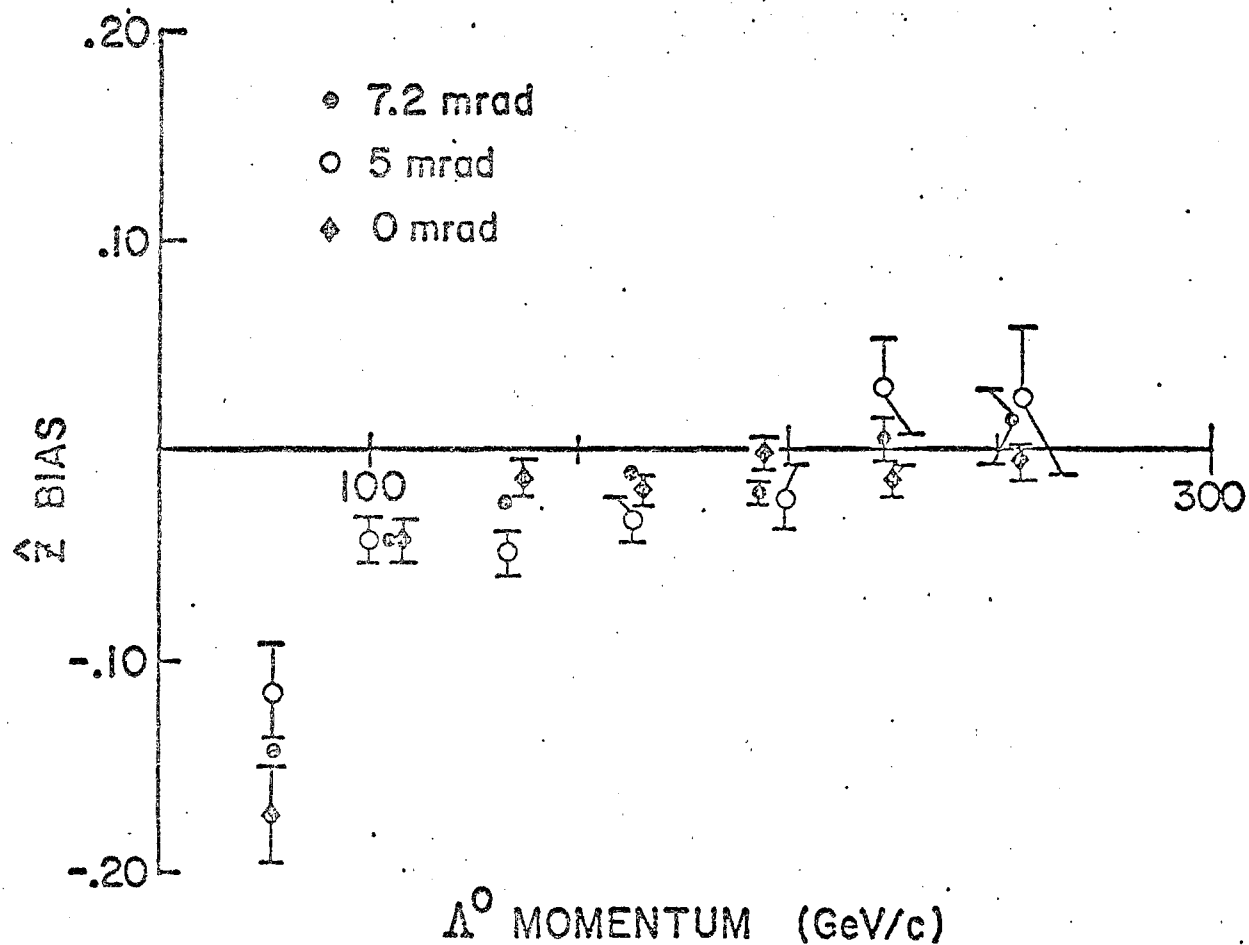


Figure 3.15b. The z bias (B) for 0, 5 and 7.2 mrad.

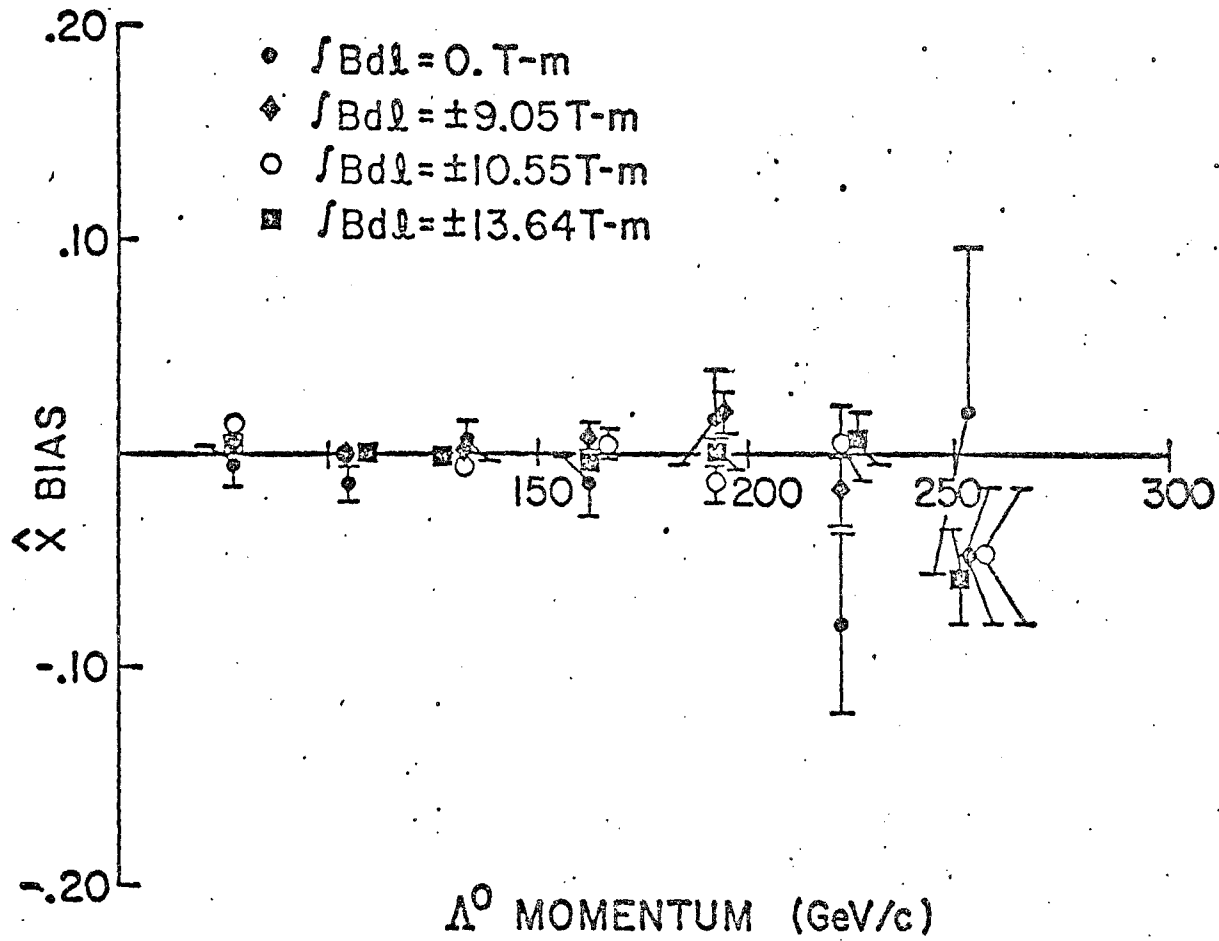


Figure 3.16a The x bias (B) for all field integrals.

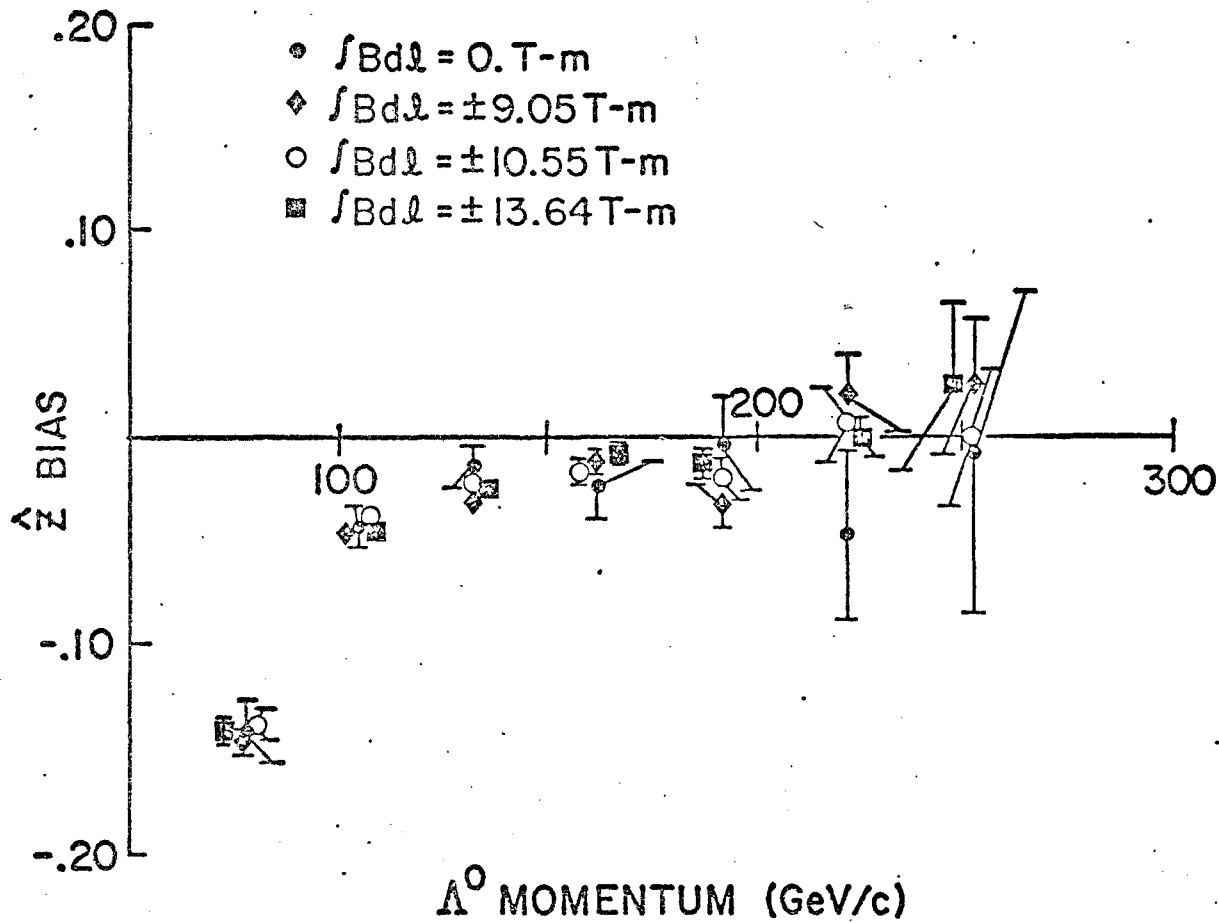


Figure 3.16b The z bias (B) for all field integrals.

This bias was unchanged by the reversal of any of the three experimental magnetic fields. The second, the spectrometer magnet bias A, reversed sign when the spectrometer magnet polarity was reversed. This bias could be cancelled simply by combining equal amounts of data taken with the two spectrometer magnet polarities. In practice, both biases A and B were incorporated into the precession analysis as parameters in a least squares fit, as described below.

3.5 PRECESSION ANALYSIS

The x and z polarization components, as calculated from Eqn. 2 can be used to calculate a precession angle for each field integral value

$$\theta = \tan^{-1}(\alpha P_z / -\alpha P_x)$$

The results of this calculation are shown in figure 3.17. The χ^2 for these points to fall on the straight line in the figure is 5.9/5 degrees of freedom. Large, uncanceled biases would cause a poor fit.

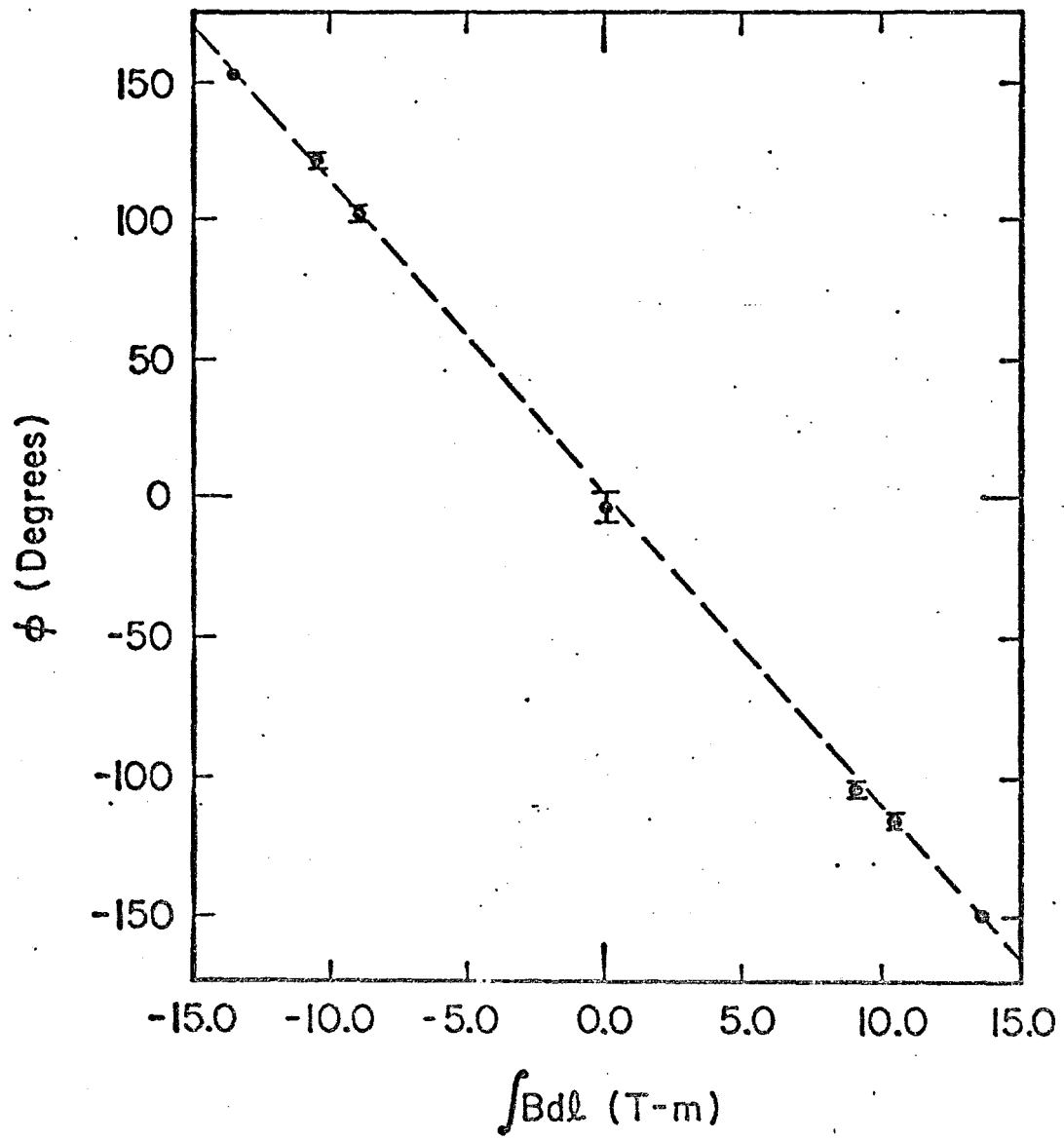


Figure 3.17 The precession angle versus field integral.

Alternatively, a χ^2 can be constructed

$$\chi^2 = \sum_{ijk} \frac{(\alpha P_{xijk} - B_{xi} \mp A_{xi} \mp \alpha P_{oi} \cos \theta_j)^2}{\sigma_{xijk}^2} + \frac{(\alpha P_{zijk} - B_{zi} \mp A_{zi} \mp \alpha P_{oi} \sin \theta_j)^2}{\sigma_{zijk}^2}$$

where $i=1,7$ runs over 7 momentum bins, $j=1,7$ over 7 field integrals, and $k=1,4$ over spectrometer magnetic field + and -, and production angle + and -. The polarization P_{oi} changes sign with production angle, the upper sign is taken for positive production angles. B_{xi} and B_{zi} are biases which are cancelled by reversing the production angle and are a function only of momentum. A_{xi} and A_{zi} are spectrometer magnet biases. The upper sign is taken for field positive. The seven precession angles, θ_j , are not parameters, but are all computed from a single parameter, the magnetic moment, through the relation, $\theta_j = 18.30 \times \int B dl_j \times \mu_N$ in degrees. P_{xijk} and P_{zijk} are the data points in 7 momentum bins for 7 sweeper field integrals, and for + and - production angle and + and - spectrometer field. Three hundred ninety two data points were used, with statistical errors σ_{ijk} . The values of the parameters from the fit are given in table 4.1. Figure 3.9 shows P_{oi} , figure 3.11 shows B_{xi} and B_{zi} .

Figure 3.18 shows A_{xi} and A_{zi} . The fit gave $\mu_{\Lambda} = -0.6138 \pm 0.0047$ n.m.. χ^2 was 380/356 degrees of freedom. The acceptable χ^2 confirms, within statistical uncertainties, the assumptions that all biases are time-independent, that they are independent of sweeper current, that the biases cancel, and that the the initial polarization was along $-\hat{x}$.

Taking data at seven field values allowed lower order ambiguities in the precession angle to be eliminated. These ambiguities take the form $\phi' = \phi + (2n+m)$ ($m=0$ or 1 , n is any integer), the two angles being indistinguishable in the measurement of ϕ at one field integral. The index, m , represents lack of knowledge of the initial polarization direction, measured by turning the precession field off. The measurements at seven field integrals exclude all values of n less than 6 and greater than -6 except $n=0$. The lowest order ambiguous solution would require $\mu_{\Lambda} = 12.40$ n.m.. This is excluded by earlier experiments.

The momentum dependence of the magnetic moment, another test of bias cancellation, was obtained by performing this fit for each momentum bin separately. The results are shown in figure 3.19. The χ^2 for these points to be equal at $\mu_{\Lambda} = -0.6138$ is 1.64. Since the

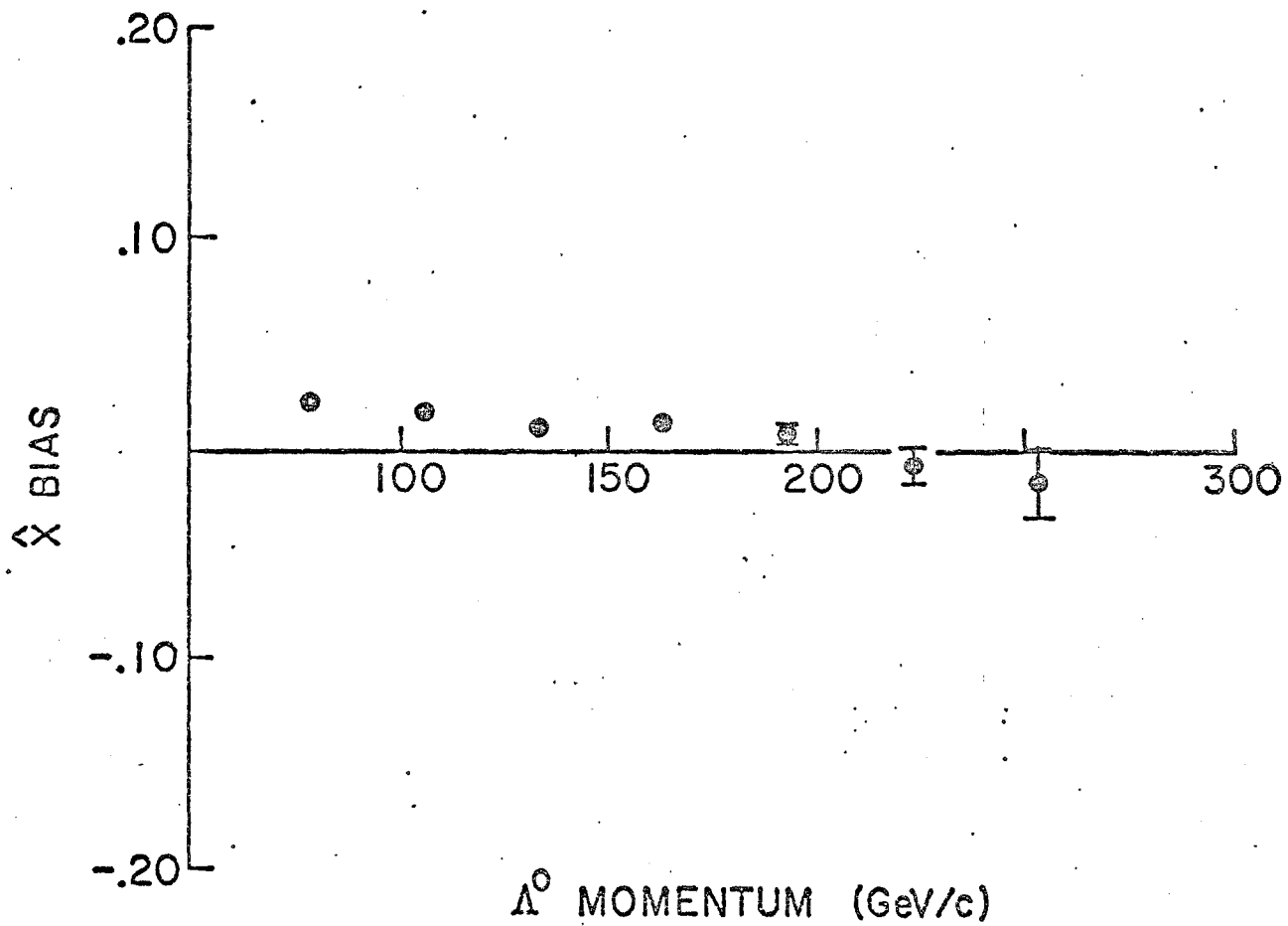


Figure 3.18a The x spectrometer magnet bias (A).

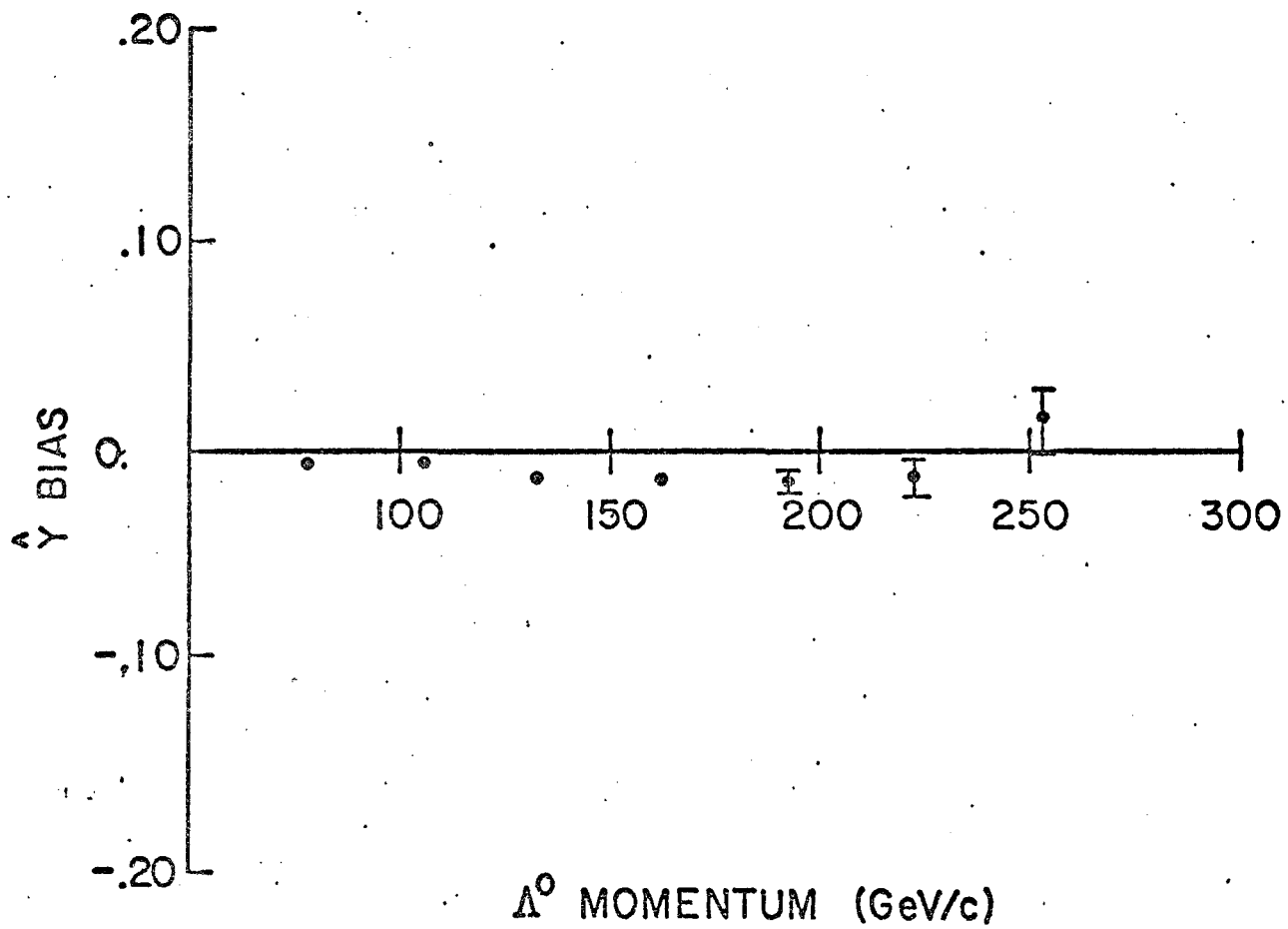


Figure 3.18b The γ spectrometer magnet bias (A).

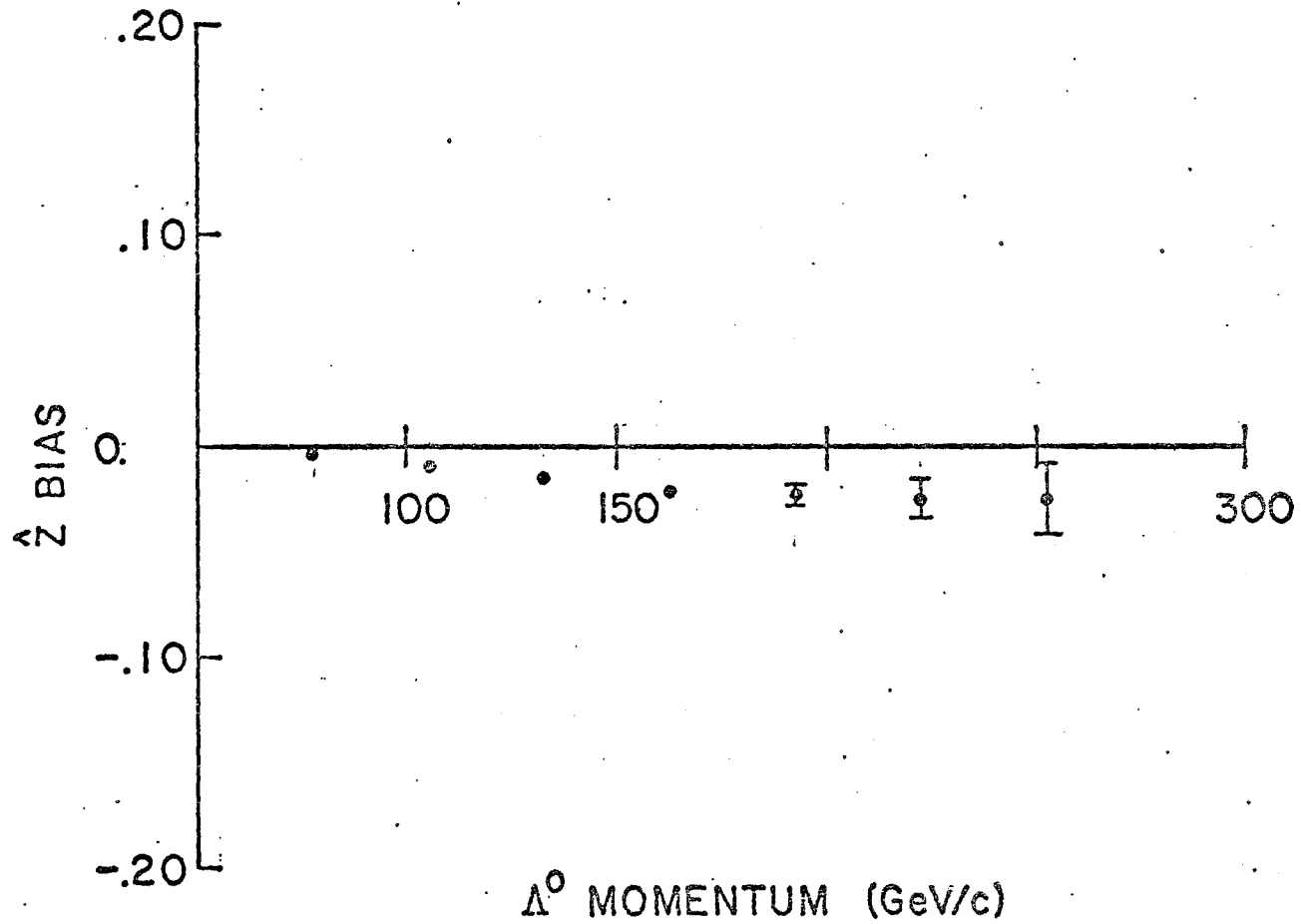


Figure 3.18c The z spectrometer magnet bias (Δ).

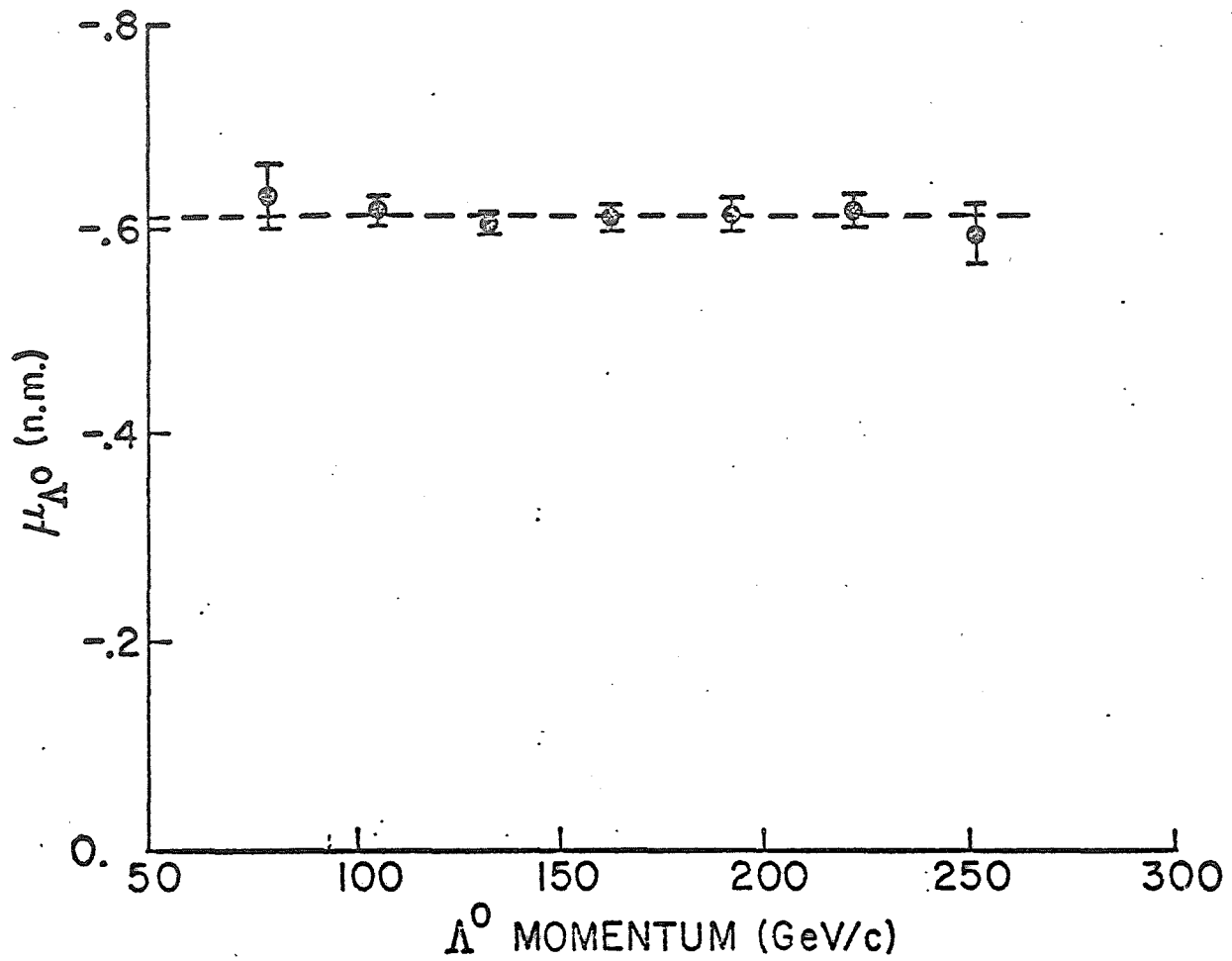


Figure 3.19 The magnetic moment versus momentum.

biases and acceptance are momentum dependent, the momentum independence of the magnetic moment is strong evidence that biases have cancelled.

3.6 SYSTEMATIC EFFECTS AND BACKGROUNDS

The stability of the magnetic moment against the variation of several cuts was tested by computing the moment for relaxed cuts. This tested for possible influences on the results of several backgrounds in the sample such as K_S^0 's, Λ^0 's from the decay $\Xi^0 \rightarrow \Lambda^0 \pi^0$, and Λ^0 's produced in the collimator.

The R^2 and θ_y cuts (see section 3.2) were varied and the magnetic moment was calculated for four conditions. The θ_y cut changed the magnetic moment by less than 0.3σ . The change in μ_Λ when the R^2 cut was broadened from 40 to 100 mm^2 was 0.6σ (0.8σ) with (without) the θ_y cut. All four results were within 0.9σ of the $R^2 < 40$, θ_y cut result.

Events which fit both the Λ^0 and K_S^0 mass hypotheses were retained as Λ^0 's. Inclusion of these events introduced a contamination of approximately 0.5% K_S^0 's. Although these events are unpolarized they can

simulate a polarization since they fall in selected regions of the $\cos \theta^*$ distribution when misidentified as Λ^0 's. These events were subtracted from the data sample by subtracting the $\cos \theta^*$ distributions for an unpolarized sample of ambiguous decays from the Λ^0 sample, with a weight of 0.5%. This was done for all three directions and all 7 momentum bins. The result quoted above includes this correction, which changed the magnetic moment by less than 0.1σ , and improved the agreement of the $\cos \theta_R^*$ with the $\cos \theta_{MC}^*$ distributions by removing the excess due to the K_S^0 contamination.

Ξ^0 decays posed a more difficult problem. If Ξ^0 's produced inclusively are polarized the Λ^0 's from the decay would display the Ξ^0 magnetic moment. The Ξ^0 moment has not been measured, nor has any inclusive polarization search been done. From previous measurements in the neutral hyperon beam it was known that the Ξ^0/Λ^0 ratio was approximately 1% at 7.2 mrad if no cut on R^2 at the production target was made. Since Ξ^0 decay produces Λ^0 's in the decay volume, most of the Λ^0 's do not point back to the production target within the required 40 mm^2 . The cut on θ_y (the angle of the Λ^0 with respect to the neutral beam in the yz plane)

also reduced the number of Ξ^0 's. An estimate of the contamination of the Λ^0 sample from Ξ^0 decay after these two cuts is 0.1%.

Another background was due to Λ^0 's produced by neutrons in the collimator. If neutrons produced inclusively are polarized, and if these neutrons produce polarized Λ^0 's near 0 degrees, the apparent magnetic moment of the Λ^0 's would be approximately -1.3 n.m. due to the combined effects of neutron and Λ^0 spin precession in the field. This would put the Λ^0 spin vector after precession in the same quadrant as that of the Λ^0 's from Ξ^0 decay if the broken SU(6) predictions for the Ξ^0 moment are correct.

In an attempt to correct for both these effects (if present) a term was added to the χ^2 which behaved like $P_{\Xi^0} \cos \theta_{\Xi^0} (\sin \theta_{\Xi^0})$ in the x (z) term. The starting value for the parameter " μ_{Ξ^0} " (μ_{Ξ^0} and/or the weighted average of μ_n and μ_p) was -1.2 n.m.. The change in the magnetic moment of the Λ^0 was 0.1σ for $R^2 < 40 \text{ mm}^2$. The difference between the magnetic moment for $R^2 < 40$ and $R^2 < 100$ was reduced to 0.1σ (0.4σ) with (without) the θ_y cut. The parameters " μ_{Ξ^0} " and " P_{Ξ^0} " were -1.38 ± 0.07 n.m. and -0.0034 ± 0.0010 from the fit with $R^2 < 100$, without the θ_y cut. The result reported here does not

include this correction.

3.7 PARITY VIOLATING POLARIZATION

A search was done for a parity violating component of polarization by adding a term to the overall χ^2 which behaved like a z component (along the average Λ^0 direction) at the production target, and was precessed by the sweeping magnet using the Λ^0 magnetic moment, which was fit simultaneously. This component was defined as positive along $+\hat{z}$, for both production angle signs. The results are shown in figure 3.20.

3.8 5 MRAD POLARIZATION

Analysis of the two data tapes taken at 5 mrad yielded the polarization shown in figure 3.21. The magnetic moment calculated from these data is $\mu_{\Lambda} = -0.597 \pm 0.017$ n.m., statistically independent of, but consistent with the 7.2 mrad result. It has not been included in the final result.

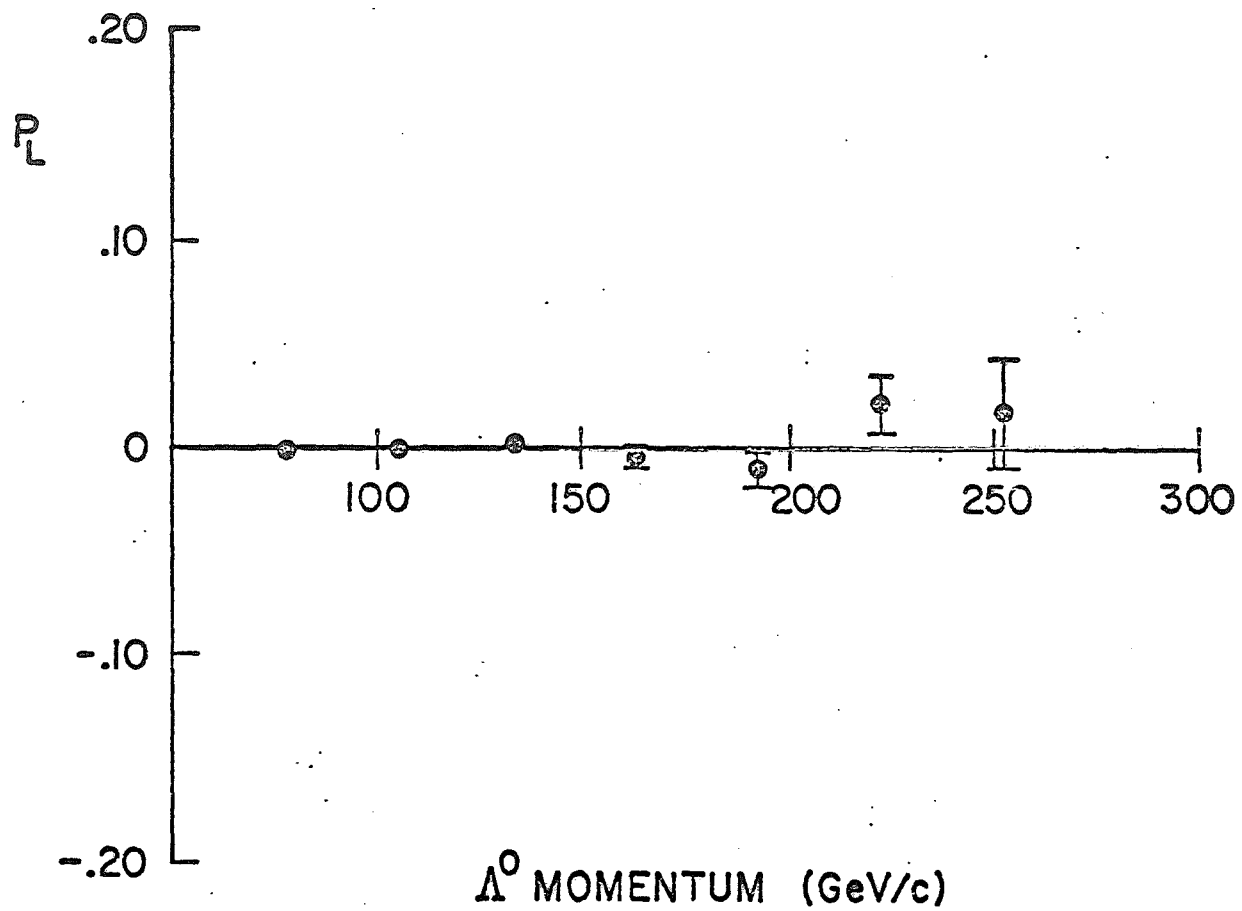


Figure 3.20 The longitudinal parity violating polarization.

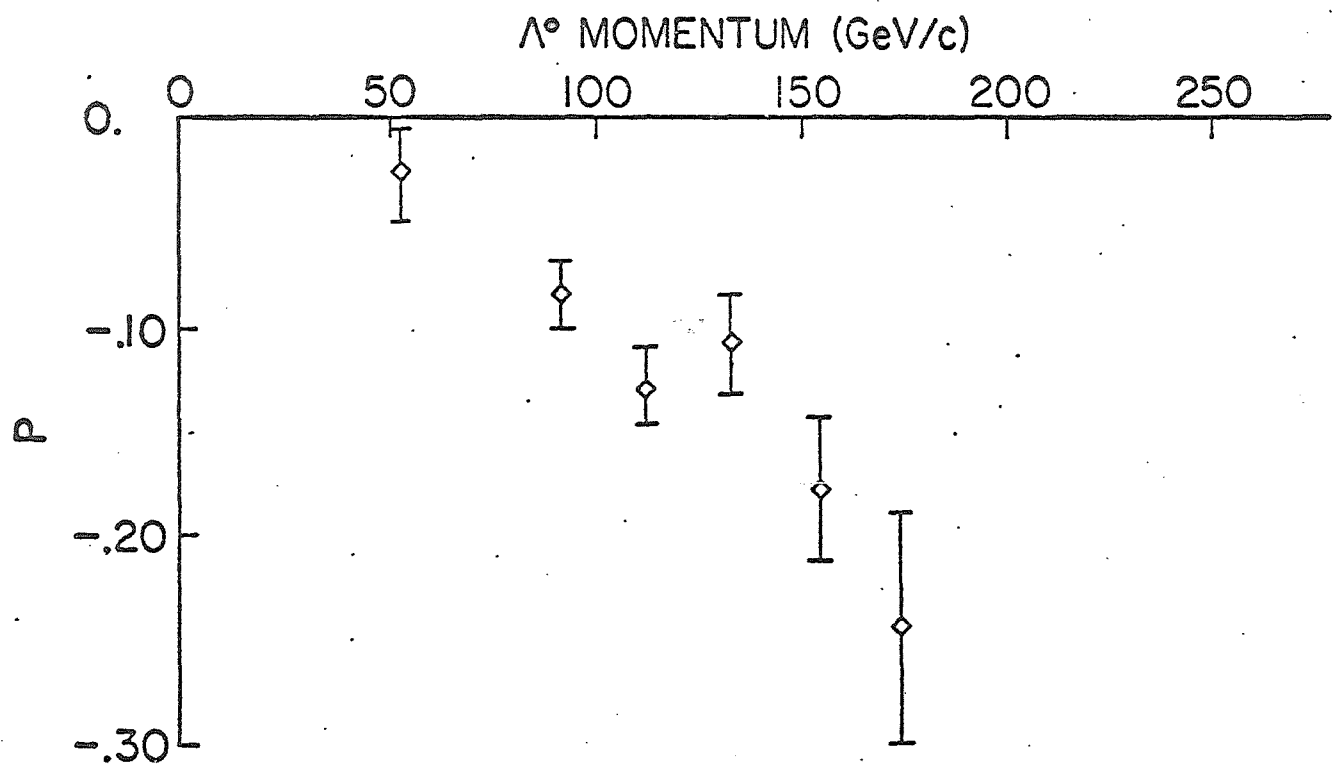


Figure 3.21 The 5 mrad polarization.

CHAPTER 4

RESULTS

4.1 MAGNETIC MOMENT

The magnetic moment of the Λ^0 hyperon has been measured to be

$$\mu_{\Lambda^0} = -0.6138 \pm 0.0047 \text{ n.m.}$$

The quoted uncertainty is statistical. Systematic uncertainties are estimated to be less than and of the order of the statistical uncertainty. A comparison with earlier measurements was shown in figure 1.1.

4.2 POLARIZATION

The parity allowed polarization of Λ^0 's produced by 400 Gev protons on Be at 7.2 mrad lab angle is shown in figure 3.9, and is listed in table 4.1.

P Gev/c	$\alpha_{P_{0i}}$	A_{xi}	A_{zi}	B_{xi}	B_{zi}
77	-0.022 ± 0.002	0.024 ± 0.002	-0.003 ± 0.003	0.005 ± 0.002	-0.141 ± 0.003
105	-0.045 ± 0.002	0.019 ± 0.002	-0.009 ± 0.002	-0.001 ± 0.002	-0.043 ± 0.002
133	-0.067 ± 0.002	0.010 ± 0.002	-0.014 ± 0.002	-0.002 ± 0.002	-0.025 ± 0.002
163	-0.090 ± 0.003	0.014 ± 0.003	-0.020 ± 0.003	0.003 ± 0.003	-0.011 ± 0.003
192	-0.117 ± 0.005	0.007 ± 0.005	-0.024 ± 0.005	0.003 ± 0.005	-0.020 ± 0.005
222	-0.135 ± 0.009	-0.008 ± 0.009	-0.026 ± 0.009	-0.002 ± 0.009	0.004 ± 0.009
252	-0.144 ± 0.017	-0.015 ± 0.017	-0.028 ± 0.017	-0.049 ± 0.017	0.011 ± 0.017

$$\mu_{\Lambda} = -0.6138 \pm 0.0047$$

$$\chi^2 = 380.4$$

392 data points

36 parameters

356 degrees of freedom

$$P(\chi^2) = 0.18$$

Table 4.1. The Λ^0 magnetic moment, polarization, and biases as a function of momentum.

The parity violating components, P_y and P_z , are shown in figures 3.14 and 3.20. They are consistent with zero. If averaged over all momentum bins these results are

$$P_y = 0.0006 \pm 0.0017$$

$$P_z = -0.0023 \pm 0.0017$$

The results as a function of momentum are listed in tables 4.2 and 4.3. Results for the polarization at 5.0 mrad are shown in figure 3.22 and listed in table 4.4.

Momentum(Gev/c)	x'	p _t (Gev/c)	Polarization
77	0.19	0.55	-0.003±0.004
105	0.26	0.75	-0.003±0.003
133	0.33	0.96	0.001±0.003
163	0.41	1.17	-0.005±0.005
192	0.48	1.38	-0.009±0.008
222	0.56	1.60	0.021±0.014
252	0.63	1.81	0.009±0.025

Table 4.2 The z parity violating polarization

Momentum(Gev/c)	x	p_t (Gev/c)	Polarization
77	0.19	0.55	0.003 ± 0.004
105	0.26	0.75	0.003 ± 0.003
133	0.33	0.96	-0.002 ± 0.003
163	0.41	1.17	-0.001 ± 0.005
192	0.48	1.38	-0.007 ± 0.008
222	0.56	1.60	0.009 ± 0.013
252	0.63	1.81	-0.017 ± 0.024

Table 4.3 The γ parity violating polarization

P Gev/c	x	P _t	POLARIZATION
77	0.20	0.39	-0.026±0.023
105	0.27	0.53	-0.034±0.015
133	0.34	0.67	-0.084±0.015
163	0.41	0.82	-0.148±0.019
192	0.48	0.97	-0.129±0.024
222	0.56	1.11	-0.179±0.035
252	0.63	1.26	-0.249±0.055

Table 4.4. The 5 mrad polarization

4.3 SUMMARY

The magnetic moment of the Λ^0 hyperon has been measured to 0.8%. Parity allowed polarization of Λ^0 's inclusively produced by 400 Gev protons rises monotonically to a value of $P = 0.22$ at a transverse momentum of $p_t = 1.81$ Gev/c. Parity forbidden components of the polarization were found to be zero at a level of 0.2%. The magnetic moment was discussed in terms of a broken SU(6) quark model, and predictions were made for a number of other baryon magnetic moments.

APPENDIX

COORDINATE SYSTEM

The z axis of the coordinate system was defined by transmitting the proton beam through the collimator (with field off) aperture and recording the chamber coordinates. The x and y axes were defined by the wires in the proportional chambers themselves. The horizontal wires measured the y coordinate and the vertical wires the x coordinate of the charged tracks. The position $x=y=0$ was the position at which the proton beam passed through the chambers.

The collimator was removed and the proton beam was transmitted through the sweeping magnet aperture, passing through the chambers at the same positions as with the collimator in place. The axis of the neutral beam at 0 mrad production angle was in this same direction to within 0.1 mrad, the angular resolution of the spectrometer for Λ^0 's.

The proton beam was then deflected with each of the three magnetic fields (production target bending magnets, sweeping field, and spectrometer field) to check that each of these fields was along an axis of the coordinate system (\hat{x} , \hat{y} , \hat{z} , respectively). The results are listed in Table A.1.

MAGNET	θ_x (mrad)	θ_y (mrad)	$\int B dl$ (T-m)
M1	-0.085 ± 0.011	1.666 ± 0.009	2.22 ± 0.01
M1	-0.083 ± 0.014	-1.647 ± 0.014	-2.20 ± 0.02
M2	8.330 ± 0.043	-0.006 ± 0.018	11.11 ± 0.06
M2	-10.040 ± 0.020	0.035 ± 0.012	-13.40 ± 0.03
M3	1.78 ± 0.07	-0.006 ± 0.015	2.40 ± 0.10

Table A.1 The angles through which the proton beam is bent. M1 is the production target bending magnet, M2 is the sweeping/precession magnet, and M3 is the spectrometer magnet.

The field integrals listed in the table are calculated using the measured angles and the beam momentum (400 Gev/c). They all agree with the measured field integrals in these magnets within errors.

Thus no significant deviation of M2 and M3 from a pure y field was seen. M1 has a small but significant bending power in the \hat{x} direction. This could contribute to the y bias which does not affect the magnetic moment measurement.

REFERENCES

1. μ_p and μ_e E. R. Cohen and B.N. Taylor, J. Phys. Chem. Ref. Data 2, 663, 1973
2. μ_n V. W. Cohen, N. R. Corngold, and N. F. Ramsey, Phy. Rev. 104, 283, 1956
3. μ_μ J. Bailey, K. Borer, F. Combley, H. Drumm, C. Eck, F. J. M. Farley, J. H. Field, W. Flegel, P. M. Hattersley, F. Krienen, F. Lange, G. Petrucci, E. Picasso, H. I. Pizer, O. Runolfsson, R. W. Williams, and S. Wojcicki, Phys. Letters 55B, 420, 1975
4. μ_{Σ^+} N. Doble, K. Gottstein, T. Hansl, I. Herynek, A. Manz, J. Marrafino, W. Matt, R. Settles, G. Wolf, E. Dahl-Jensen, I. Dahl-Jensen, S. Reucroft, C. E. Roos, J. Waters, and M. S. Webster, Phys. Letters 67B, 483, 1977
5. μ_{Σ^-} B. L. Roberts, C. R. Cox, M. Eckhause, J. R. Kane, R. E. Welsh, D. A. Jenkins, W. C. Lam, P. D. Barnes, R. A. Eisenstein, J. Miller, R. B. Sutton, A. R. Kunselman, R. J. Powers, Phys. Rev. Letters 32, 1265, 1974
6. μ_{Ξ^-} average of
G. McD. Bingham, V. Cook, J. W. Humphrey, O. R. Sander, R. W. Williams, G. E. Masek, T. Maung, H. Ruderman, Phys. Rev. D1, 3010, 1970

R. L. Cool, G. Giacomelli, E. W. Jenkins, T. F. Kycia, B. A. Leontic, K. K. Li, J. Teiger, Phys. Rev. D10, 792, 1974

7. $\Sigma^0 \rightarrow \Lambda^0 \gamma$ F. Dydak, F. L. Navarra, O. E. Overseth, P. Steffen, J. Steinberger, H. Wahl, E. G. H. Williams, F. Eisele, C. Geeniger, K. Kleinknecht, H. Taureg, G. Zech, Nucl. Phys. B118, 1, 1977

8. R. L. Cool, E. W. Jenkins, T. F. Kycia, D. A. Hill, L. Marshall, R. A. Schluter, Phys. Rev. 127, 2223, 1962

9. W. Kernan, T. B. Novey, S. D. Warshaw, A. Wattenberg, Phys. Rev. 129, 870, 1963

10. J. A. Anderson and F. S. Crawford, Phys. Rev. Letters 13, 167, 1964

11. G. Charriere, M. Gailloud, Ph. Rosselet, R. Weill, W. M. Gibson, K. Green, P. Tolun, N. A. Whyte, J. C. Combe, E. Dahl-Jensen, N. T. Doble, D. Evans, L. Hoffmann, W. T. Toner, W. Pueschel, V. Scheuing, Nuovo Cimento 46A, 205, 1966

12. E. Dahl-Jensen, N. Doble, D. Evans, A. J. Herz, U. Liebermeister, Ph. Rosselet, C. Busi, G. Onengut, P. Tolun, M. Gailloud, R. Weill, G. Hansl, A. Manz, W. Pueschel, R. Settles, G. Baroni, G. Romano, V. Rossi, Nuovo Cimento 3A, 1, 1971

13. D. A. Hill, K. K. Li, E. W. Jenkins, T. F. Kycia, H. Ruderman, Phys. Rev. D4, 1979, 1971

14. G. Bunce, R. Handler, R. March, P. Martin, L. Pondrom, M. Sheaff, K. Heller, O. Overseth, P. Skubic, T. Devlin, B. Edelman, R. Edwards, J. Norem, L. Schachinger, P. Yamin, Phys. Rev. Letters 36, 1113, 1976
15. K. Heller, O. E. Overseth, G. Bunce, F. Dydak, H. Taureg, Phys. Letters 68B, 480, 1977
16. See for example J. J. J. Kokkedee, The Quark Model, Benjamin, New York, 1969
17. A. deRujula, H. Georgi, and S. L. Glashow, Phys. Rev. D12, 147, 1975
18. E. Allen, Phys. Letters 57B, 263, 1975
19. P. L. Skubic, Ph.D. dissertation, University of Michigan Technical Report, UMHE-77-32, 1977
20. P. Martin, Ph. D. dissertation, University of Wisconsin, 1977
21. P. Skubic, O. E. Overseth, K. Heller, M. Sheaff, L. Pondrom, P. Martin, R. March, R. Handler, G. Bunce, P. Yamin, L. Schachinger, J. Norem, R. T. Edwards, B. Edelman, and T. Devlin, University of Wisconsin preprint C00-881-22, submitted to Physical Review D.
22. O. E. Overseth and R. F. Roth, Phys. Rev. Letters 19, 391, 1967

Lindsay Carol Schachinger

1969-1971 Attended Syracuse University, Syracuse, New York.
 1971-1973 Attended Douglass College, New Brunswick, New Jersey; Majored in Physics.
 1973 B.A., Douglass College.
 1973-1978 Graduate work in Physics, Rutgers University, New Brunswick, New Jersey.
 1973-1975 Teaching Assistantship, Department of Physics.
 1975-1976 Research Assistantship, Department of Physics.
 1976 Article: " Λ^0 Hyperon Polarization in Inclusive Production by 300 Gev Protons on Beryllium," Physical Review Letters, Vol. 36, p. 1113.
 1976-1977 University Fellowship, Rutgers University.
 1977 Article: "Inclusive Production of Neutral Strange Particles at 300 Gev: Triple Regge Behavior," Nuclear Physics, Vol. B123, p. 1.
 1977 Article: "Inclusive Production of Hyperons by 300 Gev Protons: A Dependence," Physical Review, Vol. D16, p. 2737.
 1977-1978 Research Assistantship, Department of Physics.
 1978 Article: "Hyperon Polarization in Λ^0 -p Elastic Scattering in the Range 60 Gev/c $< p < 380$ Gev/c," Physical Review Letters, Vol. 40, p. 491.
 1978 Article: "Forward Inclusive Production Spectra of K_s^0 , Λ^0 , $\bar{\Lambda}^0$, and n in the Collision of 200 Gev π^- , K^- , p, and \bar{p} on Be," Physical Review D, Vol. 18, p. 76.
 1978 Article: "Polarization of Lambdas and Antilambdas Produced by 400 Gev Protons," Physical Review Letters, Vol. 41, p. 607.
 1978 Ph. D. in Physics.

